Thermodynamics and Structure-Property Relationships of Charged Block Polymers

Bradley J. Grim, Matthew D. Green*

Chemical Engineering, School for Engineering of Matter, Transport and Energy, Arizona State University, Tempe, AZ 85287
E-mail: mdgreen8@asu.edu

Keywords: block polymers, structure-property relationships, self-assembly, phase behavior, polymeric electrolytes, secondary interactions

Abstract

Advancements in electronics and energy storage and conversion technologies brings with it myriads of exciting material design challenges. Charge-containing block polymers offer unique features which can overcome some of these challenges and have thus aroused substantial interest within the field of designer soft materials. The properties of block polymers are intricately coupled to the dynamic and rich nature of the nanostructured assemblies which result from the phase separation between blocks. The introduction of strong secondary forces, such as electrostatics and hydrogen bonding, into block polymers greatly influences their self-assembly behavior, and therefore affects their physical and electrochemical properties often in non-trivial ways. In this review, we present some of the prevailing research which has expanded our understanding of structure-property relationships to include several design strategies for improving ionic conductivity and modulus in charged block polymers. We also highlight the profound extent to which electrostatics and hydrogen bonding impact block polymer thermodynamics, an extent which has been demonstrated by recent theoretical and experimental work. Insights gained from the research presented here help to lay the groundwork for a long and bright future in the field of advanced soft materials.

1. Introduction

Charge-containing polymers are used in a diverse array of applications, consequently making them a prominent area of research for the past several decades. Batteries,[1–3] fuel cells,[4–6] actuators and transducers,[7–15] and separation membranes[16–20] are among the continually growing list of useful applications investigated, most of which require dimensional stability. The introduction of charges into polymeric materials often impairs mechanical integrity, depending on the environmental conditions and electrostatic interaction strength, which can result in undesirable aqueous dissolution or brittleness. In addition, electrolytic homopolymers are, in general, inherently weak since charge transport necessitates either chemical/segmental mobility[21] or charge dense ion-hopping pathways.[22] Both transport mechanisms provide ion-solvation-site connectivity[23] but correlate to low glass transition temperatures and elastic moduli. Some approaches for overcoming this hurdle are to mix rigid polymers with ionic liquids (ILs),[23] cross-link,[24] add inorganic supports,[25] use block polymer architectures,[1,4] or simply limit charge content. Each of these methods possess its own pros and cons and are all worth pursuing; however, one aspect that limits them all is the tradeoff between mechanical integrity and operational performance. Block polymers (BPs) have a tendency to phase separate into periodic assemblies, which allows one to decouple mechanical integrity and operational performance by independently tuning the characteristics of a particular microdomain. For block polymer electrolytes (BPEs), one domain provides a structural framework while the other provides an interconnected ionic matrix.

The extent to which polymers are insoluble with each other, also known as their segregation strength, is denoted by the thermodynamic term χN, where χ is the Flory-Huggins interaction parameter and N is the number of repeat units. When χN is large enough, unfavorable mixing interactions between blocks force them to phase separate while covalent bonding between blocks limits their diffusion to the local interface, resulting in periodic morphologies on the nano- to micro-length scale.[26] An incredibly vast library of morphologies has been captured over the years with their geometric complexity increasing in conjunction with number of blocks, block architecture/configuration, processing conditions, and the number of chemical constituents.[27,28] However, the most common morphologies observed for BPs are lamellar (LAM), gyroid (GYR), hexagonally packed cylinders (HEX), body centered cubic spheres (BCC), and disordered (DIS). One which is less common, but still relevant is hexagonally perforated layers (HPL). The fashion by which every unique BP system self-assembles defines its phase behavior which, in the

simplest case, is influenced by volume fraction (i.e. composition, *f*), and degree of polymerization (N). While our understanding of self-assembly for neutral BPs has been well-established, both experimentally and theoretically, the introduction of electrostatics and other secondary interactions (e.g. hydrogen bonding and π-π stacking) has been shown to drastically complicate the thermodynamics, often shifting the order-disorder transition (ODT) and order-order transition (OOT) boundaries around the *f*-χN phase diagram. The degree to which this happens is highly dependent on the chemical nature of the charged groups and their connectivity within the material. The enthalpic and entropic contributions of charges in BP thermodynamics envelopes numerous elements which are all highly correlated, making it especially difficult to draw generalizable conclusions about the impacts of individual factors. Coupling each thermodynamic contribution to its performance impact further complicates this picture, especially when equilibrium is brought into question. Myriad examples show that morphology and its constituent components, such as tortuosity and interfacial width, all play an important role in dictating transport performance in BPs. Harnessing control over the charge-morphology-property relationships for charged BPs is essential for the effective design and development of advanced soft materials and will thus be the focal point of discussion in this review. To elucidate these connections across literature, theoretical and experimental work must be sewn together. Thankfully, significant progress has been made within each field to provide a clearer understanding.

The predictive and insightful guidance from theoretical and computational investigation is invaluable. The level of control and modulation over independent variables along with a high level of detail encompassing the data grants direct correlation between cause and effect, at least within the accessible range of the model. Theoretical models often comprise necessary simplifying assumptions brought about either by computational constraints or for the purpose of providing generalizable predictions. Reality, however, makes no assumptions and can be incredibly laborious to simplify, especially in fields such as functional polymer physics where the parameter space is vast. This lack of simplicity convolutes comparisons between studies which often differ by several variables within the parameter space. Examples include *charge* type, connectivity, distribution, and mobility, and *backbone* chemistry, composition, molecular

weight, dispersity, and configuration. Additionally, charged BPs are often plagued by insufficient equilibration bound by degradation and/or slow kinetics, further complicating their comparison. Although it is difficult to isolate and observe the effects of a single thermodynamic influence, there are sufficient studies within the field to elucidate the impacts of several general parameters, and hence provides the motivation for this review.

2. Morphology, Ion Correlations, and Material Performance

This section will primarily focus on the coupling between BP phase thermodynamics and performance measures in general. For comprehensive reviews on charged polymers for specific applications or reviews on specific types of charged polymers, the reader is directed elsewhere.[2–4,6,7,10,18,19,25,28–40]

High ionic conductivity is one of the most common central goals encompassing electrolytic design. Historically, there has been a tradeoff between conductivity and mechanical strength for BPEs[41] but there have been substantial efforts to find support blocks which contribute to ion transport. The well-known lithium-ether complexation makes ether-based polymers ideal candidates for applications in cation transport with poly(ethylene oxide) (PEO) being the most extensively studied.[36,42] PEO is often tethered to polystyrene (PS) or poly(methyl methacrylate) (PMMA) support blocks and doped with lithium salts including lithium bis(trifluoromethanesulfonyl)imide (LiTFSI) or lithium perchlorate ($LiClO_4$). There are alternative platforms which offer notable cation transport properties (Mindemark/Brandell 2018), although their salt-induced thermodynamic behavior in BPEs are less understood than that for PEO. Several hurdles still exist for ether-based BPEs that limit their use in commercial battery applications such as insufficient conductivity which is further impaired by PEO crystallization, low Li transference number (i.e. high anion mobility), and their inability to completely inhibit Li dendrite growth in Li-metal batteries (Maslyn/Balsara 2018).[43] Inhibition of dendritic growth in Li-metal batteries is influenced both by anion mobility[44] and modulus,[45] which if rectified will enable the next generation of high energy density batteries.[46–48] Other performance measures besides conductivity stand out in different applications such as capacitance in polymer actuators,[14] chemical/thermal stability, and fuel permeance (e.g., too low in the electrode

ionomer[49,50] or too high in the electrolyte membrane)[51]) in polymer electrolyte membrane fuel cells. Creative approaches for improving these performance measures in BPEs are widespread throughout the literature, however, the question is: How are these measures related to or effected by morphological characteristics?

2.1. Molecular weight, composition, and charge content

Molecular weight (MW), composition, and charge content are the simplest and most direct routes for tuning the properties in any given BPE system, but there are tradeoffs for each. We start by using Li-salt doped PS-PEO as an example. Charge content, commonly defined as the ratio of Li cations to ether segments (r = [Li]/[EO]), has been shown to maximize conductivity (at 90 °C) in the vicinity of $r \approx 0.1$ in PEO homopolymer, considered as the percolation threshold where cooperative segmental motion starts to become hindered.[52,53] In symmetric PS-PEO, however, conductivity has shown a bimodal dependance on salt content (Figure 1c) with the first maxima occurring at $r \approx 0.1$ and the second at $r \approx 0.2$ with conductivity being greater in the latter ratio.[54] This phenomenon is believed to be caused by a reduction in grain boundary size with increasing r which exemplifies the interdependent relationships between charge content, morphology, and conductivity.

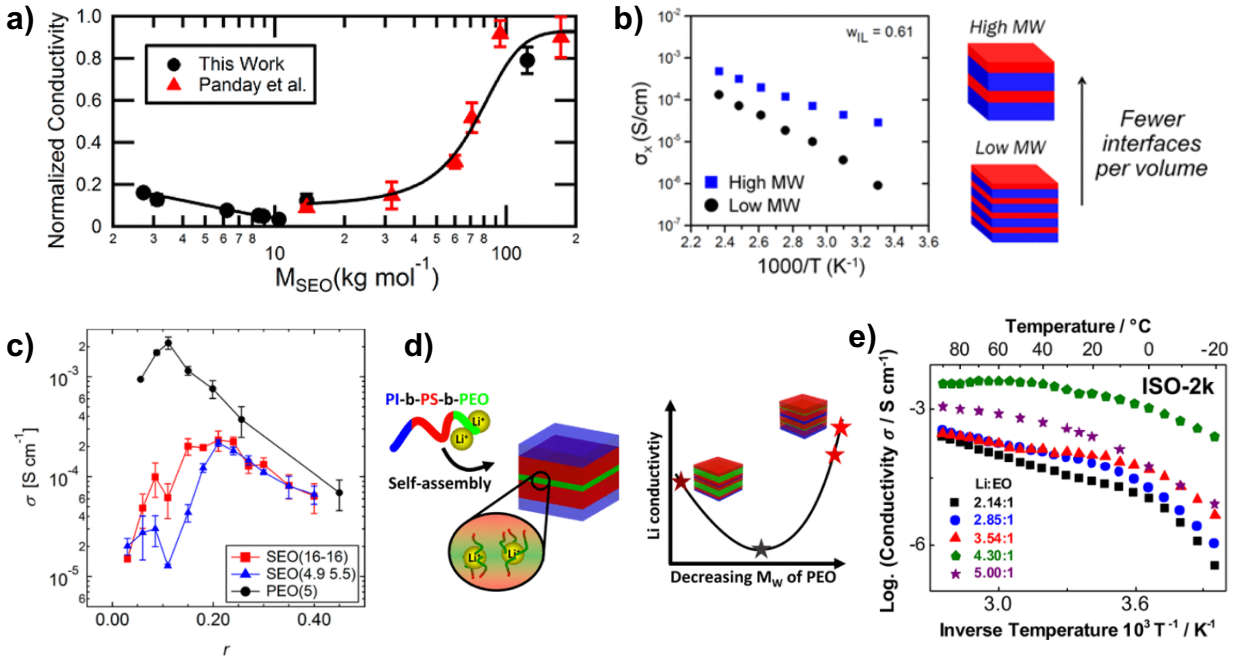

Figure 1. (a) Dependence of conductivity on molecular weight (M_{SEO}) for symmetric PS-b-PEO/LiTFSI at r = 0.085. Adapted with permission.[59] Copyright 2013, American Chemical Society. (b) PS-b-PMMA mixed with an IL at an IL weight fraction (w_{IL}) of 0.61. Adapted with permission.[56] Copyright 2016, American Chemical Society. (c) Conductivity at 90 °C of two LAM-forming PS-PEO/LiTFSI BPs as a function of salt content as compared to PEO/LiTFSI homopolymer. Adapted with permission.[54] Copyright 2016, American Chemical Society. (d) Illustration showing the relationship between conductivity and PEO molecular weight for LiTFSI-doped PI-b-PS-b-PEO (ISO) where (e) the highest conductivities were obtained at the lowest PEO molecular weight studied (2 kg/mol) and a doping ratio of r = 4.30 (green pentagons). Adapted with permission.[62] Copyright 2019, American Chemical Society.

Balsara and coworkers found that increasing molecular weight improves conductivity in symmetric PS-PEO/LiTFSI above 10 kg/mol (Figure 1a).[53,55] Comparable findings were observed for IL-doped PS-PMMA (Figure 2b).[56] The opposite trend has been observed for LiTFSI-doped PEO homopolymer wherein increasing PEO molecular weight was shown to diminish conductivity.[57] Ion transport in BPs is thought to reduce at the block interface due to insulating effects from the support block.[58] Hence, this discrepancy can be explained by a decrease in interfacial surface area density with increasing molecular weight, thus reducing the fraction of ions effected by interfacial insulation from the support block.[56] Decreasing the molecular weight of PS-PEO/LiTFSI below 10 kg/mol was later found to invert the conductivity-molecular weight relationship wherein conductivity increases with decreasing molecular weight

(Figure 1a).[59] Reducing molecular weight to such an extent for BPs is however detrimental to their real-world application since glass transition temperature (T_g) and modulus begin to decrease rapidly as molecular weight decreases below the entanglement threshold.[60] Pelz et al. were able to bypass these low molecular weight restrictions by introducing a third block (polyisoprene (PI)) to control self-assembly in PI-PS-PEO and found that minimizing PEO molecular weight strongly benefits total conductivity, allowing for superior conductivity >10^{-3} S/cm down to 0 °C with a surprisingly minimal temperature dependence and a Li/EO ratio of r = 4.3 (Figure 1d,e).[61,62] Additionally, Li transference number in this sample was found to be 0.70 which is significantly higher than that measured in PEO/LiTFSI (< 0.4).[63] For comparison, the conductivity of 5 kg/mol PEO/LiTFSI up to r = 0.45 is shown in Figure 1c (black) which exhibits a declining trend with respect to increasing r. This discrepancy indicates a considerable shift in the ion transport mechanism which the authors ascribed as a decoupling between Li transport and backbone segmental motion, commonly believed to be the primary cation transport mechanism in polyethers.[64]

2.2. Tapering

Block polymer tapering is defined by a monomeric concentration gradient (A→B) between neighboring blocks which can be conceptualized as a separate, interfacial block characterized by its size and direction (normal = A-b-(A→B)-b-B, and inverse = A-b-(B→A)-b-B). An illustration of block tapering can be found in Figure 11b. Tapering the transition between blocks can improve BPE performance on multiple levels. Kuan et al. were the first to introduce BP tapered into BPEs which, most notably, improved Li conductivity by 90-190% between 80-20 °C, respectively, over the non-tapered counterpart while maintaining well-defined morphologies.[65,66] On a mechanistic level, normal-tapering is able to reduce chain stretching, thus improving segmental mobility at the domain interface. This relief of packing frustrations at the interface was also shown to stabilize network morphologies which are beneficial for ion transport.[67] Additionally, by controlling the size and direction of the tapered segment, they were able to reduce χ_{eff} which is especially useful for reducing melt processing temperatures. The combined improvement in conductivity and reduced segregation strength signifies tapering to be

a promising factor for developing BPEs and deserves further investigation. Ketkar et al. has recently compiled an Account which includes the research described above[68] in addition to a detailed review on Li-ion polymer electrolytes.[31]

2.3. Terminal functionality

Improving cation transference (i.e., reducing anion mobility) in cation exchange BPEs is equally beneficial to electrolytic performance as conductivity. One method for doing this is to introduce hydrogen bond donors which can interact/complex with anions, thus limiting their mobility. Jung et al. found that substituting the terminal hydroxyl (-OH) group of PEO in nearly symmetric PS-PEO (f = 0.46) with mono- and di-functional -OH and carboxylic (-COOH) acids has significant impacts on its mechanical and transport properties (Figure 2a-e).[69] Substitution from mono- to di-functional acids increased storage moduli by 3-7x and corresponded to a LAM→GYR transition (beneficial for transport). At low LiTFSI content of r = 0.02, all acid substitutions were able to greatly suppress PEO crystallization (Figure 2c). The impact of end-group type on Li transference number is displayed in Figure 2d with -OH producing a more favorable impact than -COOH. The addition of an extra terminal -OH increased Li transference nearly 2-fold at 60 °C due to increased hydrogen bonding with the anion. Complementary data for the di-functional -OH showed a 47% decrease in anion diffusivity for r = 0.02 and an even larger decrease of 72% for r = 0.06, both at 50 °C. This was better achieved by -OH than -COOH since hydrogen bonding weakens with increasing acidity. Although total conductivities between mono- and di-functional -OH systems did not differ much above $T_{m,PEO}$, the transference-number-corrected conductivities would have shown proportional improvements. Increasing salt content to r = 0.06 from 0.02 reverted both diacid GYR morphologies back to LAM which are generally less desirable than GYR in electrolytic applications depending on grain size.[70] More recently, Kim et al. utilized terminal nitrile ($-C \equiv N$) functionalities to improve the performance of PS-b-PEO/PEO blend electrolytes doped with LiTFSI.[71] By tuning the degree of nitrile functionality on the BP and the homopolymer, they effectively enhanced several performance measures including conductivity, Li transference, electrochemical stability, and even modulus. Given the vast library of accessible end-group chemistries, coupled with its high impact on material

performance, terminal functionality in BCEs will likely receive considerable attention in the coming years.

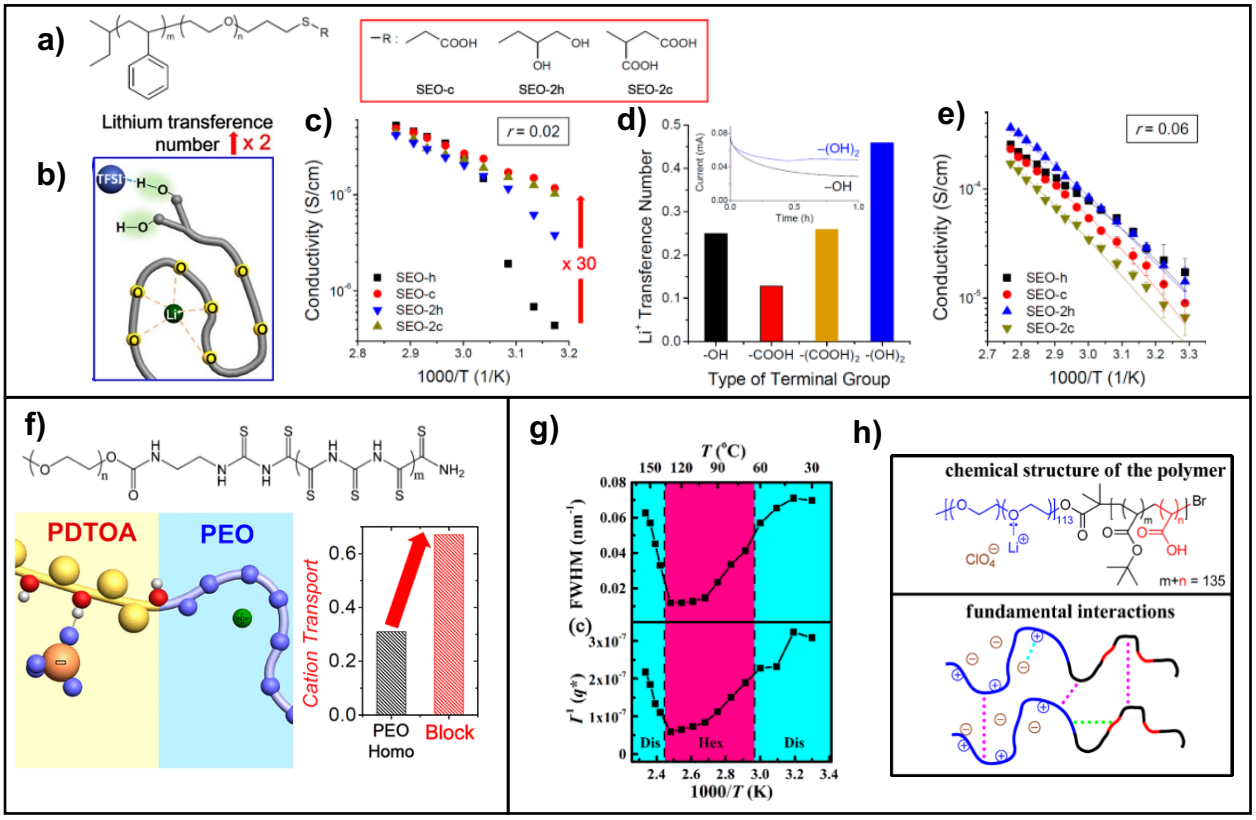

Figure 2. Properties and characteristics of block polymers with H-bond functionalities. (a) Chemical structure of PS-PEO with mono- and di- acid terminal functionalities with a (b) illustration of interactions when doped with LiTFSI. (c) Arrhenius conductivity trends show that PEO crystallization can be suppressed with -COOH end-group functionality at low salt doping. (d) Li transferrence as a function of end-group type showing -OH the be more effective than -COOH at improving Li transferrence while increasing the number of end-groups can improve further improve Li transferrence. (e) Arrhenius conductivity trends at higher salt loading (r = 0.06) shows higher conductivity than for r = 0.02 and a complete suppression of PEO crystallization regardless of eng-group type. Adapted with permission.[69] Copyright 2017, American Chemical Society. (f) Chemical structure of poly(ethylene oxide-b-dithiooxamide) (PEO-b-PDTOA) and illustrations showing how H-bonding interactions between the support block (PDTOA) and anions can improve cation transferrence by increasing ion-pair dissociation. Adapted with permission.[75] Copyright 2015, American Chemical Society. (g) Temperature-variable SAXS data for the chemistry in (h) shows the possible closed-loop phase behavior which can result from alike systems where competitive electrostatic and H-bonding interactions exist. Adapted with permission.[76] Copyright 2018, American Chemical Society.

2.4. Conductivity-contributing support blocks

Many support blocks such as PS yield insulating effects on conductivity caused by a combination of low segmental motion and a lack of solvation sites.[58] For this reason, it is imperative for us to find support phases which contribute to the ion transport mechanism in some way. One route is simply finding support blocks that contain solvation sites. The Li salt-induced effects on PEO-based BPEs with a conducting support phase (poly(propylene monothiocarbonate), PPMTC) was studied by Cao et al. with the goal of improving both mechanical integrity and conductivity simultaneously.[72,73] Although the secondary conducting phase studied was an amorphous, low T_g (~0 °C) polymer, their findings should be transferrable to alike systems with competing ion solvation preference between phases. At lower salt concentrations, preferential ion solvation into the PEO phase initially induced microphase separation with no ODT observed up to 100 °C, while at higher concentrations, ion translational entropy resulted in mixing, consequently diminishing mechanical integrity.[72,73] It should be noted that salt concentrations in this study spanned much higher than most (up to r = 1/3), and only at the highest concentration did mechanical strength diminish completely. Between Li doping ratios of r = 1/24, 1/12, and 1/6, the transitions noted were DIS→LAM→DIS respectively. However, the DIS states were still weakly phase separated, evidenced by a single small-angle X-ray scattering (SAXS) peak, with storage moduli closely resembling that of their ordered LAM sample. With conductivity for the ordered LAM sample surpassing 10^{-4} S/cm above 50 °C at r = 1/6 (equivalent to PS-PEO/LiFTSI at 90 °C, Figure 1c) while maintaining a useful storage modulus, this method shows promise for electrolytic applications. Another unique feature of these BPEs was the relative insensitivity of ordering to variations in temperature, with no stark transitions occurring between 30-100 °C, suggesting that competitive ion-backbone interactions can broaden the ODT boundary. In summary, the introduction of a conducting support block into BPEs can improve conductivity while consequently resulting in non-monotonic trends in χ_{eff}, and thus modulus, with salt loading. Modulus, however, might be improved through choice of semicrystalline poly(monothiocarbonate) analogues.[74] Although the crystalline nature of these analogues may be compromised by the addition of salts just as the crystallinity of PEO decreases with LiTFSI loading.

Another approach for improving ion transport contributions from the support block is to introduce hydrogen bond (H-bond) donors which, like that observed by Jung et al. previously,[69] have been found to improve Li transference via anion complexation. Jo et al. probed this

approach by using a polydithiooxamide (PDTOA) support block attached to PEO and were able to effectively isolate some of the ClO_4^- counterions of Li salts (up to $r = 0.09$) into the support phase via H-bonding (Figure 2f) without noticeably affecting the morphology. This resulted in a normalized conductivity of ~ 0.8, surpassing the theoretical limit of 0.66 for LAM morphologies,[75] and leads to an interesting question of how non-covalent coercion of the anion into the support phase affects BP thermodynamics. Wang et al. may have answered this question by doping $LiClO_4$ into a poly(ethylene oxide)-b-poly(t-butyl acrylate-co-acrylic acid) diblock terpolymer (Figure 2g,h), likely coercing the ClO_4^- anion into the support phase via hydrogen bonding. Although there were no characterizations showing ClO_4^- behavior or specific mention of acid-perchlorate interactions, the BP thermodynamics observed were incredibly exciting.[76] For the first time, closed-loop phase behavior was observed in strongly interacting BPs where both an upper order-disorder transition (UODT) and a lower disorder-order transition (LDOT) occurred within the same system (Figure 2g). Increasing acid content decreased segregation strength while subsequent doping with $LiClO_4$ increased it. Hence, greater acid content required greater $LiClO_4$ to induce phase separation while further increasing both consequently inverted morphological temperature trends into LDOT behavior. Fourier transform infrared (FT-IR) spectroscopy trends in C=O stretching for the acrylic acid group established relative evidence of both ether-hydrogen bonding and Li-ether complexation but it is unclear how much, if any, acid-ClO_4^- interactions existed. These interactions may improve electrical properties as they did in Ref.[69], however, being able to tune the phase behavior to such a degree could prove revolutionary in the advancement of BPEs. Two important aspects to note between using an amide versus more acidic groups to provoke anion hydrogen bonding is their differences in hydrogen bond donor strengths and ability to chelate or form dentated complexes. Higher proton-base dissociation lowers potential binding energies for acids whereas secondary amides are characteristic of strong hydrogen bond donors with high pKa values and are commonplace in dentated polymers and chelating agents.

2.5. Single-ion conductors

While both ion and counterion contribute to the overall conductivity of an electrolyte, it is only advantageous in many electrolytic applications for one of the ions to migrate. The ion which does not contribute to electrolytic performance will herein be referred to as the subordinate ion and the other as the primary ion. Fixing the subordinate ion to the backbone is considered one of the most efficient methods for improving transference of the primary ion. Thus, these so-called single-ion conductors have attracted considerable attention. Ryu et al. may have been the first to find in BPEs that covalently tethering the subordinate Li counterions into a secondary phase (a non-primary conducting phase) can increase the Li transference number nearly to unity due to increased ion pair dissociation.[77] The BPE of inquiry was poly(lauryl methacrylate-*co*-Li methacrylate)-*b*-poly(oligo oxyethylene methacrylate) where Li methacrylate groups were randomly distributed along the lesser conducting backbone. SANS and AFM data showed some evidence of phase separation that lacked a well-defined morphology which can also be described as random or disordered concentration fluctuations. However, no ODT measurements were conducted and only a single T_g was observed which was interpreted as comparable shifts in domain T_gs due to Li and methacrylate ion pairs dissociated between phases. Bouchet et al. extended the previous work by attaching a trifluoromethanesulfonylimide (TFSI analogue) anion to styrenic monomers (PSTFSILi), to make PSTFSILi-b-PEO-b-PSTFSILi triblock copolymers, improving upon several BPE performance measures over the LiTFSI doped PS-PEO-PS counterpart including transference number, conductivity, and even modulus to a substantial degree.[78] Using a lower molecular weight diblock copolymer form of this system (Figure 3a), Balsara and coworkers probed in more depth the morphology-property relationship.[79,80] They observed DIS→LAM transitions driven by PEO crystallization for 7.0, 8.2, and 9.0 kg/mol BPs with 29, 39, and 44 wt% PSTFSILi, respectively, which supports claims of phase separation by Bouchet below the melting temperature of PEO. All phase separated samples in Figure 3b contained ionic clusters sequestered in the PSTFSILi phase at 25 °C implying a lack of ion-pair dissociation although clustering seemed to be suppressed at the lowest charge content. Conductivities measured for DIS samples at 90 °C (Figure 3b) were nearly identical to those measured by Ryu et al. at the same charge composition (17 wt% PSTFSILi) implies that the chemically equivalent BPs investigated in both studies were DIS above the PEO melting temperature. Since then, several other analogous BPEs have been studied, all so far resulting in mixed and/or crystallization induced LAM.[81–86] A more detailed discussion on the

thermodynamic nature of these systems can be found in section 3.1. It is, however, important to note here that χ was estimated to be negative for PEO-PTFSILi in most cases,[83] implying that demixing for this system may be either unattainable or incredibly difficult without some additional thermodynamic driving force such as crystallization. Stabilizing the morphology in single-ion conducting BPEs such as these may be attainable via addition of a third block. A third block might also provide an avenue for drastically reducing the molecular weight of PEO just as Pelz et al. did with PI-PS-PEO (Figure 1d,e).[62]

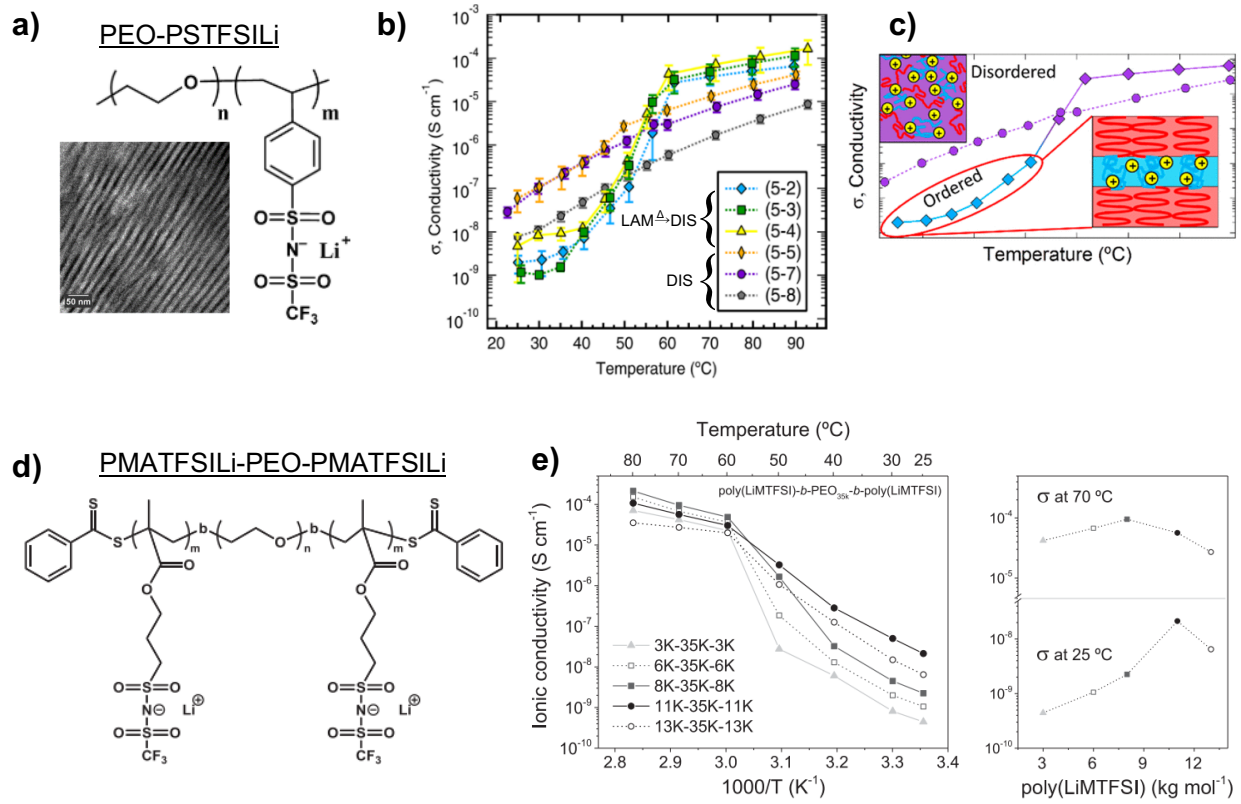

Figure 3. (a) Chemical structure of TFSI-pendant PS-PEO and inset micrograph showing its LAM morphology (8.2 kg/mol, f_{PEO} = 0.69). (b) Conductivity vs. Temperature for PEO-PSTFSILi with PSTFSILi molecular weights ranging from 2-8 kg/mol and PEO molecular weight of 5 kg/mol. (c) Illustrative explanation of the conductivity behavior shown in (b). Adapted with permission.[79,80] Copyright 2014, 2015, American Chemical Society. (d) Chemical structure of PMATFSILi-PEO-PMATFSILi triblock copolymer. (e) Arrhenius plot of conductivity for PMATFSILi-PEO-PMATFSILi with PMATFSILi molecular weights ranging from 3-13 kg/mol and a PEO molecular weight of 35 kg/mol. Conductivities at 25 °C and 70 °C are shown as a function of PMATFSILi molecular weight. Adapted with permission.[81] Copyright 2017, Elsevier.

2.6. Nano-confinement and normalized conductivity

Conductivity of the ionic phase has been shown in a few instances to be even higher in BPEs than in their fully charged, homopolymer (normalized conductivity, $\sigma_{norm} > 1$). This phenomenon signifies either a shift in the transport mechanism and/or a decrease in the activation energy for ion transport due to the confinement of charges. This resembles a study previously discussed (Figure 1d,e).[61] To calculate σ_{norm} for the system shown in Figure 1d,e, we would need to know the conductivity of PEO/LiTFSI at $r = 4.3$. Assuming PEO/LiTFSI retains only a single maximum in conductivity at $r \sim 0.1$ (Figure 1c), then σ_{norm} would have likely shown >> 1, especially since their highest measured conductivity came from a sample with only 4 vol% PEO. Further investigation into alike BPEs is hugely warranted.

Elabd and coworkers observed $\sigma_{norm} > 3$ for hydrated imidazolium-functional anion exchange BPEs (with Br^- or OH^- counterions) even though water uptake was higher in the homopolymer equivalent.[87,88] Additionally, Kim. et al. showed an order-of-magnitude improvement in conductivity over the homopolymer analogue for sulfonic acid-functional, anhydrous proton exchange BPEs doped with imidazolium-type ILs.[89] More recent work compared Li conductivity trends between styrene-based IL-functional BPEs and the charged homopolymer counterparts which were strikingly similar, indicating a $\sigma_{norm} \sim 1$.[90] Although the measured conductivity was high, Li transference was negative in all cases, implying that conductivity was heavily dominated by anion mobility.[90,91] Regardless, these studies all suggests that charge confinement into percolating domains has great potential for improving transport properties beyond current theoretical limits. The four aforementioned studies involved ILs which transport ions through a segmental motion-assisted, ion hopping mechanism wherein the ion hopping mode improves with respect to decreasing backbone-backbone distance while the segmental motion mode remains correlated to T_g.[92] Conceptually, this is interpreted as reducing the hopping distance between solvation sites, in turn reducing the activation energy barrier required to move the ion from one site to the next. Hence, if solvation site spacing can be reduced without significantly increasing the T_g, then conductivity performance will enhance, and it seems that nanoscale confinement in BPEs is able to achieve this goal under certain conditions. Such conditions would likely only occur at high charge content, a regime which has been shown to reduce domain spacing with increasing salt content regardless of electrostatic strength.[93] Nano-

confinement has even led to crystalline phases in zwitterion + IL doped BPEs which were not observed in the homopolymer analogues, resulting in crystalline proton-conducting channels able to reduce polarization losses.[94]

2.7. Thermal history and non-equilibrium morphologies

True melt equilibrium morphologies are not always accessible when degredation preceeds adequate annealing temperatures.[95–97] They are sometimes not even desirable, either because thermal annealing is not cost and/or time efficient in terms of processing, or because it actually hinders material performance.[98,99] In either case, kinetically trapped morphologies are expected.

Truong et al. solution casted an ABCBA sulfonated pentablock terpolymer (NEXAR®) with an ion exchange capacity (IEC) of 2.0 meq/g from n-propanol/toluene casting mixtures and found that increasing n-propanol content (i.e., increasing polarity) of the casting solution resulted in ordered LAM between 29-36 wt% n-propanol and disordered LAM between 40-50 wt% n-propanol, with more polar solvents being less selective.[100] Broad, higher order SAXS peaks were still apparent in the samples, which they classified as disorder LAM because the diffraction patterns resembled more of a random network-like morphology. This network-like morphology likely enhanced this sample‘s water uptake and conductivity performance over the well-ordered LAM sample. Water uptake increased smoothly with casting solvent polarity (decreasing order), while proton conductivity underwent a marked step-change improvement between 2-5x in the less ordered sample. However, conductivity in the well-ordered samples showed little dependence on water uptake (10-25 wt% water). Zheng et al. observed the exact opposite trends using an identical backbone (NEXAR®) with a lower IEC of 1.2 vs 2.0 meq/g and cast from a THF/cyclohexane/heptane mixture rather than propanol/toluene.[101] Increasing polarity of the casting solvent (increasing THF) led to more ordered structures, however, higher ordering in their case corresponded to a 2-fold increase in water uptake and an order of magnitude increase in conductivity. The disordered morphologies in the latter study consisted of discrete transport domains rather than random interconnected networks observed in the preceding study, resulting in opposite order-property trends between the studies. The stark disparity in properties observed

between similar BPs cast from propane/toluene vs THF/cyclohexane/heptane mixtures denotes that polarity of the casting solvent alone is not a sufficient parameter to control self-assembly. A more fundamental understanding of the solvent-polymer thermodynamics which take place during casting would provide significant impacts within the field of BPEs.

3. Charged Block Copolymer Thermodynamics: Theory and Experiment

Because block configuration[102] and dispersity[103–107] so greatly affect phase behavior, linear diblock and triblock copolymers synthesized via controlled polymerization currently comprise most of the literature on charged BP thermodynamics. Additionally, since the neutral case for linear systems is more sufficiently established experimentally, the specific impacts of charge on phase behavior become significantly simpler to resolve. Electrostatic interactions generate a variety of effects on BP thermodynamics but can be categorized in general by their tendency to shift the phase boundaries vertically and/or horizontally along the composition-segregation strength (f-χN) phase space. The former, which consists only of vertical shifts, will be denoted here as "weakly interacting systems." The latter consisting of horizontal shifts are normally complemented with vertical shifts, although difficult to characterize in parallel, and will be denoted as "strongly interacting systems." These labels were chosen because, theoretically, significant horizontal shifts in ordered phases occur when enthalpic contributions from electrostatics are strong and dominate thermodynamic behavior.[108]

3.1. Weakly Interacting Systems

Vertical shifts in the ODT boundary are driven primarily by ion translational entropy which shifts the ODT boundary up, and preferential ion solvation which shifts it down. This corresponds to a decrease or increase, respectively, in the order-disorder transition temperature (T_{ODT}) as χ is inversely proportional to temperature in most cases and can be approximated by the expression $\chi = \chi_H/T+\chi_S$, where the subscripts represent the enthalpic and entropic terms respectively. Each component in χ is classically considered to be constant, however, this

postulate was formed by considering primary interactions alone such as van der Waals (vdW) forces, and hence neglecting the complex and dynamic nature of secondary forces.

Balsara and coworkers, along with several other groups, have extensively probed the thermodynamics of lithium (Li) salt doped polystyrene-b-polyethylene oxide (PS-PEO),[41,53,54,59,109–115] providing a wealth of information which has recently been compiled and analyzed.[112] A simplified polynomial expression with coefficients fit to Leibler's theory[116] was provided which grants facile prediction of χN or domain spacing for neat blends and BPs of PS and PEO, thus facilitating comparison between self-consistent field theory (SCFT) and calculated χ_{eff} values for individual systems. A common method for calculating χ_{eff} has been to fit SAXS data to equations developed by Leibler which have been subsequently simplified and organized by Balsara and Teran.[109] The fitting procedure is often performed using the random phase approximation (RPA) which denotes a BP transitioning into a DIS state before it is completely homogeneous, evidenced by a single scattering peak. A linear relationship between χ_{eff} and r has been obtained for several BPE systems, but this relationship often breaks down at higher salt concentrations wherein χ_{eff} saturates.[114,117,118] To better understand the phase behavior of PS-PEO/LiTFSI, a collaborative study was performed by Loo, Balsara, Hou, and Qin, with the latter two being developers of a relatively simple "free-ion" SCFT depicted in Figure 4a,b.[119,120] Experimental data for PS-PEO/LiTFSI were fit to the model described above (Figure 4c,d) using ionic solvation radius as the only fitting parameter which exists within an expression quantifying the difference in ion solvation energy between phases, $\lambda_B \equiv \frac{l_0}{2}\left(\frac{\varepsilon_A - \varepsilon_B}{\varepsilon_A \varepsilon_B}\right)\left(\frac{1}{a_+} + \frac{1}{a_-}\right)$, where l_0 is the vacuum Bjerrum length, $\varepsilon_{A,B}$ is the relative phase permittivity of phase A or B, and a_+ and a_- are the cation and anion solvation radii, respectively. Not surprisingly, the effects of salt doping in PS-PEO were found to lay comfortably in the solvation dominated regime ($\lambda_B = 5.8$) due partially to the strong dielectric mismatch between PS and PEO. The theoretical calculations qualitatively resembled the experimental data used for fitting and showed a slight asymmetric shift in ordered morphologies towards lower $f_{EO,salt}$ and r (Figure 4c,d). The resulting solvation radii fits for Li and TFSI from this model ($a_{Li} = 1.43$ nm, $a_{TFSI} = 5.43$ nm) are an order of magnitude larger than those measured for PEO/LiTFSI,[121] indicating a significant overestimation of ion solvation-induced ordering via the Born model used in their calculations. However, recent work by Qin's group[122] revealed that this

overestimation could be relieved by considering composition fluctuations, which are known to amplify the destabilization of ordered phases at lower molecular weights.[122–125]

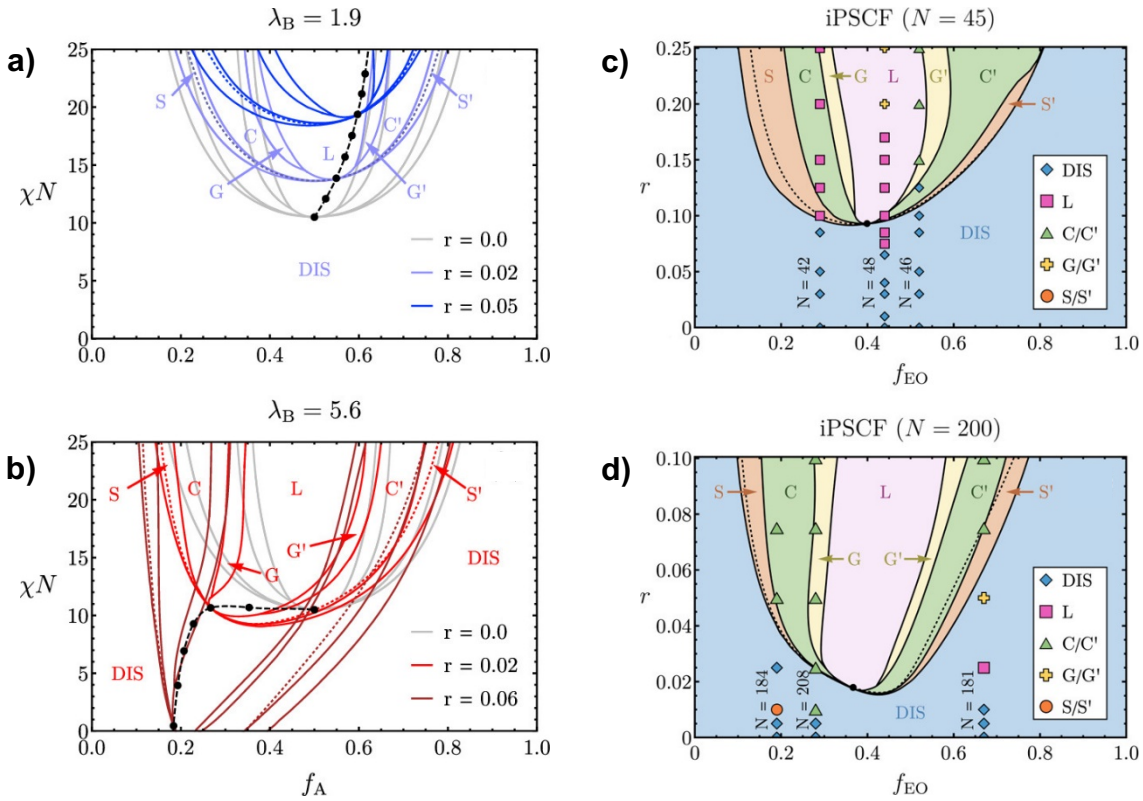

Figure 4. Salt-doped diblock copolymer phase diagrams from (a, b) unique SCFT predictions illustrate how increasing the difference in ion solvation energy between phases (λ_B) can shift phase behavior from being dominated by (a) entropic and (b) solvation effects. (c, d) The same SCFT model is fit to experimental data from PS-PEO/LiTFSI to produce phase diagrams which highlight the effects of molecular weight on phase behvior with respect to salt doping (r) and PEO/LiTFSI volume fraction (f_{EO}). Adapted with permission.[120] Copyright 2020, American Chemical Society.

In contrast, more entropy dominated systems (still weakly interacting) have been observed in salt-doped BPs where maxima in χ_{eff} were found at intermediate salt concentrations (Figure 5d) due to competitive ion interactions between blocks.[73,126–128] Several interesting thermodynamic features were apparent in $LiClO_4$-doped PEO-b-polycaprolactone (PEO-PCL)[126,127] and LiTFSI-doped PEO-b-poly(propylene monothiocarbonate) (PEO-b-PPMTC),[72,73] both of which demonstrated an unprecedented level of stabilization for LAM and HEX phases relative to PS-PEO/LiTFSI.[112] An approximate phase diagram for PCL-PEO/$LiClO_4$ is shown in Figure 5a, although the complete set of phase transitions observed by Huang et al. was significantly richer, two of which are displayed in Figure 5b. Additionally, PPMTC-PEO/LiTFSI stabilized the LAM

phase down to $f_{PEO/salt}$ = 0.275 although its phase behavior was more entropically penalized compared to PCL-PEO/$LiClO_4$ which could be a factor of higher complexation site density in PPMTC relative to PCL. The OOTs displayed in Figure 5b for $f_{PEO/salt}$ ~ 0.5 demonstrate a shift

in the ordered phases towards lower PEO compositions, a phenomenon only expected in systems exhibiting strong electrostatic cohesion.[93,129] This data signifies chain stretching to be

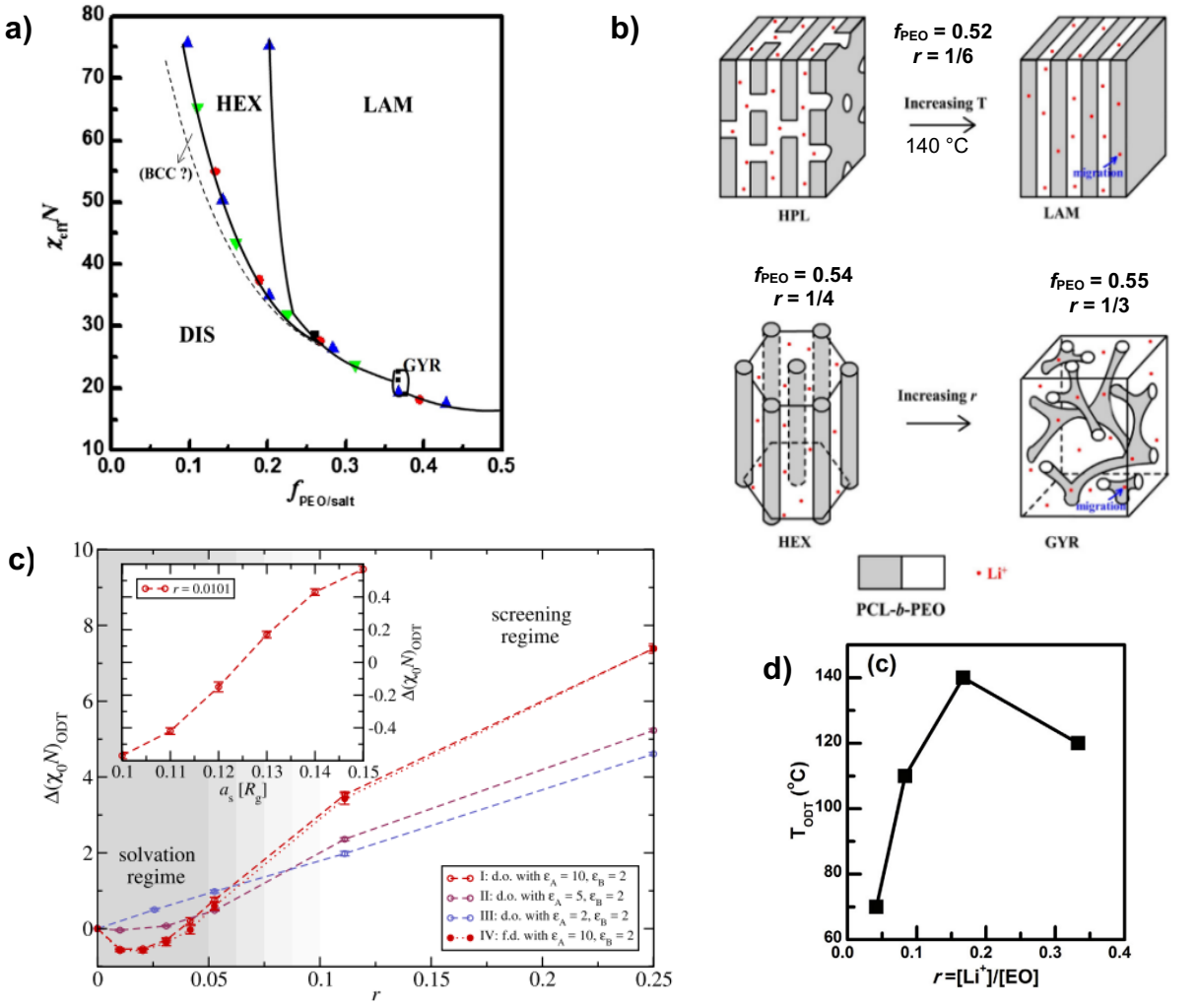

Figure 5. Experimental (a, b, and d) and theoretical (c) studies exempifying the complex nature of ion dynamics on phase behavior of systems with prominent entropic effects. $LiClO_4$-doped poly(ε-caprolactone)-b-poly(ethylene oxide) (PCL-b-PEO/$LiClO_4$) (a) Phase diagram of PCL-b-PEO/$LiClO_4$ shows a drastic stabilization of the LAM phase down to low volume fractions of the PEO block ($f_{PEO,salt}$). (b) Illustration of unexpected morphologies and ODTs for PCL-b-PEO/$LiClO_4$ at M_n ~ 10.2 kg/mol. Adapted with permission.[127] Copyright 2014, Elsevier. (c) Theoretical shifts in the ODT boundary vs. salt loading (r) for polarizable BPs with various dielectric contrasts show and initial increase in segregation strength at low r which quickly transitions to a decrease in segregation strength around $r > 0.05$. This transition corresponds to entropic screening effects overpowering enthalpic solvation effects at some intermediate salt content. Adapted with permission.[134] Copyright 2019, American Chemical Society. (d) Experimental T_{ODT}s measured for PCL-b-PEO/$LiClO_4$ show a non-monotonic trend with respect to salt content which generally resembles the behavior shown in (c). Adapted with permission. Copyright 2013, Elsevier.

significantly more prominent in PEO than in PCL, thus causing the PEO phase to consume more interfacial area. This could possibly be due in part by the ability of Li-PEO complexes to conform to rod-coil like structures with EO:Li being 6:1,[130] but this cannot be the only factor or else LAM stabilization would appear in the other PEO-based BPEs previously described. The interesting and unusual HPL→LAM OOT in Figure 5b observed upon heating is normally the inverse (LAM→HPL), otherwise the expected OOTs would be HPL→HEX or HPL→GYR. This could either be caused by a shift in composition due to ion migration or if the enthalpic and/or entropic components in $\chi = \chi_H/T+\chi_S$ were temperature dependent. Ideally, χ is reduced with increasing temperature, resulting in a decrease in the interfacial energy (e.g., LAM→HPL) as loosely described by the Helfand-Tegami and the Tang and Freed relationships for infinite and finite molecular weight polymer blends, respectively.[93,131,132] Therefore, one of the classically constant components in χ might also be temperature dependent, which results in or is caused by the migration of salts between phases.[127] If Li-ester complexes weaken with temperature faster than for Li-ether complexes, increasing temperature would enthalpically drive Li back into the PEO phase while entropy drives it the other way. Hypothetically, this could help explain the non-linearity observed between χ and 1/T for alike systems.

Recent theoretical work by Grzetic and Fredrickson provided deeper insight into the entropic nature of the experimental phenomena mentioned above by studying the salt-dependent ODT behavior of symmetric, polarizable BPs with various dielectric mismatches.[133,134] Their findings yielded a parabolic (i.e., non-linear) trend in the ODT with salt loading (Figure 5c) which correlates to a maximum in χ_{eff}, similar to that observed in PCL-PEO/LiTFSI (Figure 5d). When the dielectric contrast between phases is sufficient, preferential ion solvation into the higher dielectric domain stabilizes ordering at low salt concentrations while at higher concentrations, electrostatic screening of van der Waals (vdW) attractions leads to mixing. When the permittivity of each phase is equivalent, ions behave as a non-selective solvent, leading to a linear increase in $(\chi N)_{ODT}$ with *r*. Although the results obtained from this study are exaggerated with respect to experimental findings for systems such as PS-PEO/LiTFSI where χ_{eff} saturates with salt loading, it provides some evidence that this saturation could be influenced by preferential solvation effects being offset by electrostatic screening of vdW attractions.

In the extreme case where both counterion entropy and anti-preferential ion solvation degrades segregation strength, such as the case discussed earlier (Figure 3), phase mixing is a prevailing occurrence.[79–86] The goal for such systems is to maximize ion-pair dissociation which has been shown to improve transport properties, but by doing so increases the energies associated with mixing. Let us considering the specific case for PSTFSILi and PMATFSILi tethered to PEO (Figure 3a,d) at the ODT, all of which were ordered due to the crystallization of PEO. Upon heating (melting of PEO crystallites), Li ions are driven into the PEO phase by Li-ether interactions. Polarization at the interface caused by ion-pair dissociation presents an incredible driving force for mixing which is likely exacerbated by anion-anion repulsion within the ionic phase. While calculated χ_{eff} values for PEO-b-PSTFSILi at 29 and 39 wt% PSTFSILi were negative, χ_{eff} for the 18 wt% sample was slightly positive,[83] implying that phase separation might improve for this composition at higher molecular weights. However, the same PEO crystallization induced ODT was still observed for a compositionally equivalent triblock copolymer with a 7x greater molecular weight.[86] Replacing PEO in PMATFSILi-b-PEO with poly(oligo ethylene glycol methacrylate) (POEGMA) to eliminate the effects of PEO crystallization on phase behavior; Porcarelli et al. observed mixing in all samples across a range of compositions (15-50 wt% PMATFSILi) and relatively high molecular weights (51.5-88.0 kg/mol).[82] This finding exemplifies the extent to which mixing is preferred when counterions in one block exhibit strong enthalpic interactions with the opposing block. Exchanging Li^+ with divalent Mg^{2+} in $PSTFSI^-$-b-PEO has been the only successful demonstration for decreasing miscibility between PEO and PSTFSI blocks due to ionic cross-linking between pendant anions within the $PSTFSI^-$ phase,[83–85] and should apply to other analogous BPEs.

Introducing a tapered interfacial segment into BPEs can offset the increase in χ_{eff} with salt doping in addition to stabilizing or destabilizing certain morphologies depending on the size and direction of tapering.[65,66,135] As mentioned previously, salt loading increases segregation strength in solvation dominant BPEs while interfacial tapering produces the opposite effect. Additionally, normal-tapering (defined in section 2.2, depicted in Figure 11b) has the propensity to stabilize network structures such as GYR by relieving some inherent packing frustrations.[136] This effect was demonstrated by the observation of a double-gyroid morphology in a tapered LiTFSI-doped PS-POEGMA BPE (f_{PEO} = 0.52, 33 kg/mol, $f_{taper} \approx 0.6$) which is highly unusual for a symmetric system.

A lamellar superlattice morphology was observed for the first time by Shim et al. in charge-neutral BPs using a compositionally symmetric, relatively low molecular weight (9-10 kg/mol) PS-POEGMA backbone functionalized with pendant-Na sulfonate charges at various concentrations.[137–139] The superlattice geometry vanished at higher charge content and was also not observed after substituting the tethered charges with free salts of equivalent chemistry. Significantly larger domain sizes appeared for the salt doped system (+50%) with the calculated Bjerrum length being roughly equivalent to the observed superlattice domain spacing. The authors speculated that this superlattice behavior might reveal some sort of competitive relationship between length scales for charge cohesion and optimal chain packing.[102] They were also able to break down the superlattice domain via homopolymer doping in volumetrically symmetric equivalents, although surprisingly this did not occur until a homopolymer volume fraction > 0.2.[137] Homopolymer doping in BPs introduces space to relax chain stretching,[140–142] which could, thus, extend the system outside the competition range between the length scales mentioned previously. At higher BP molecular weights, no superlattice was observed, and the system displayed a similar morphological dependance on charge concentration (up to $[Na^+]/[EO] = 0.16$) as that of its PS-PEO/LiTFSI analogue[59] indicating that preferential ion solvation dominates thermodynamic behavior. It is however surprising that the combined effects of solvation preference and electrostatic cohesion within this system do not drastically shift the phase diagram as predicted and illustrated in Figure 8 in the following section. The authors indicated that counterion solvation effects may contribute to this mismatch. Additionally, sulfonate anions attached to the terminus of backbone oligomers still contain a relatively high degree of translational freedom as compared to other pendant charges which are confined more closely to the backbone. This extended linkage between pendent charges and the polymer backbone would manifest as an entropic penalty. A study tuning pendant charge entropy via its linkage distance from the backbone would shed light on the extent of its impacts.

3.2. Strongly Interacting Systems

Horizontal shifts in ordered phases are representative of strong electrostatic interactions which increase interfacial surface tension and result in a lower charged volume fraction that occupies

more interfacial surface area. This is sometimes described using the term “phase inversion” when the matrix/continuous phase transitions from being the volumetric majority component to being the minority component. Strong electrostatic interactions generally manifest in charge pendant systems rather than salt doped systems due to the considerable decrease in ion translational entropy and can result in phase asymmetry which defines a horizontal shifting of ordered phases along the composition axis. Phase asymmetry is generally accompanied by shifts in χ_{eff} to an extent which is highly dependent on composition. At lower charge compositions, χ_{eff} is expected to increase while the inverse is expected at higher charge compositions and is governed by counterion entropy.[93,129] The above statements assume mixing to be endothermic although exothermic mixing is possible which can potentially flip the temperature dependent mixing from an upper order-to-disorder transition (UODT) to a lower disorder-to-order transition (LDOT), akin to upper and lower critical solution temperatures, respectively. This phenomenon will be referred to herein as “boundary inversion” and does not simply manifest as a consequence of exothermic mixing which was exemplified in the previous section for PEO-b-PSTFSILi. In this section, we will focus primarily on systems where phase asymmetry and/or boundary inversion occurs.

3.2.1. Phase asymmetry

Many early studies on pendant charge effects in BPs were based on styrene sulfonate in its acidic form, likely due to synthetic simplicity and high thermal and chemical stability. Although the sulfonic acid group is not formally ionic, the high dissociation constant of the proton offers it strong electrostatic characteristics. In 2008, Park et al. conducted an in-depth thermodynamic study of compositionally symmetric poly(styrenesulfonate)-b-poly(methylbutylene) (PSS-PMB) across a wide range of molecular weights (2.8-43.6 kg/mol) and sulfonation levels along the PS backbone (0-53 mol%). Despite the compositional symmetry, a rich variety of morphologies were observed as sulfonation content increased, morphologies which were only expected at substantially higher volume fractions of PSS. This provided some of the first evidence of electrostatic effects that could not be explained using current theory at the time.[143] Goswami et al. solution casted a very similar BP in THF at room temperature to produce a phase inverted

HEX morphology with PSS forming the continuous phase although it was the volumetric minority.[144] Upon annealing the sample at 120 °C for several days, the morphology shifted from HEX to LAM, a transition which can be explained by lowering χ_{eff}. It is important to note that the PSS composition was 0.25 which still constitutes a horizontal shift in ordered phases relative to neutral BPs. Hybrid Molecular Dynamics/Monte-Carlo simulations performed by the authors mirrored their observed phase inversion from solution cast samples, suggesting that the morphology observed may not have been predominantly influenced by preferential solvation effects while casting below T_g which can result in kinetically trapped (i.e., non-equilibrium) structures. Phosphonic acid substituents have been shown to result in very similar phase behavior as that described above for sulfonic acid, with sulfonic acid generating a slightly greater increase in segregation strength (Figure 6).[145] Park and coworkers have since expanded their research on acid-tethered PS-PMB with various degrees of functionality, in addition to IL and zwitterion doping to produce a fascinating variety of morphologies and phase behaviors with relevant applications.[146,147]

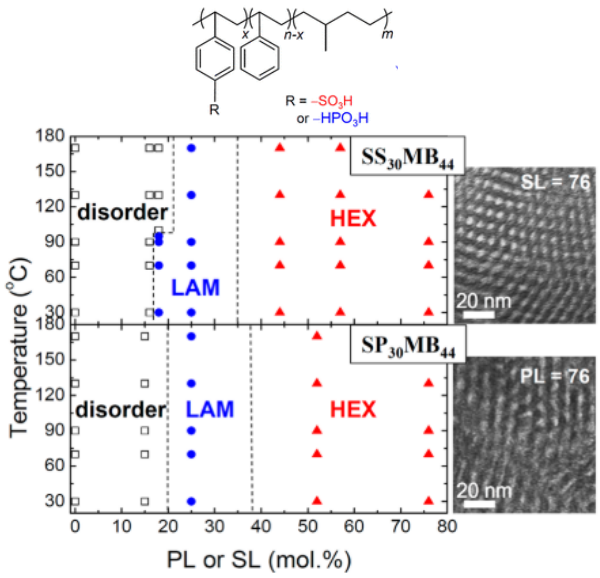

Figure 6. Phase diagrams for Poly(styrene-b-methylbutylene) bearing various levels of sulfonic (SL) or phosphonic (PL) acid along the styrenic block. With increasing acid content, the molecular weight for both BPs increases from 6.3 to 8.0 kg/mol which coincides with a volume fraction increase of the acidic block from 0.45 to 0.50 respectively. Dark portions in the TEM images on the right represent acidic domains. Adapted with permission.[145] Copyright 2015, American Chemical Society.

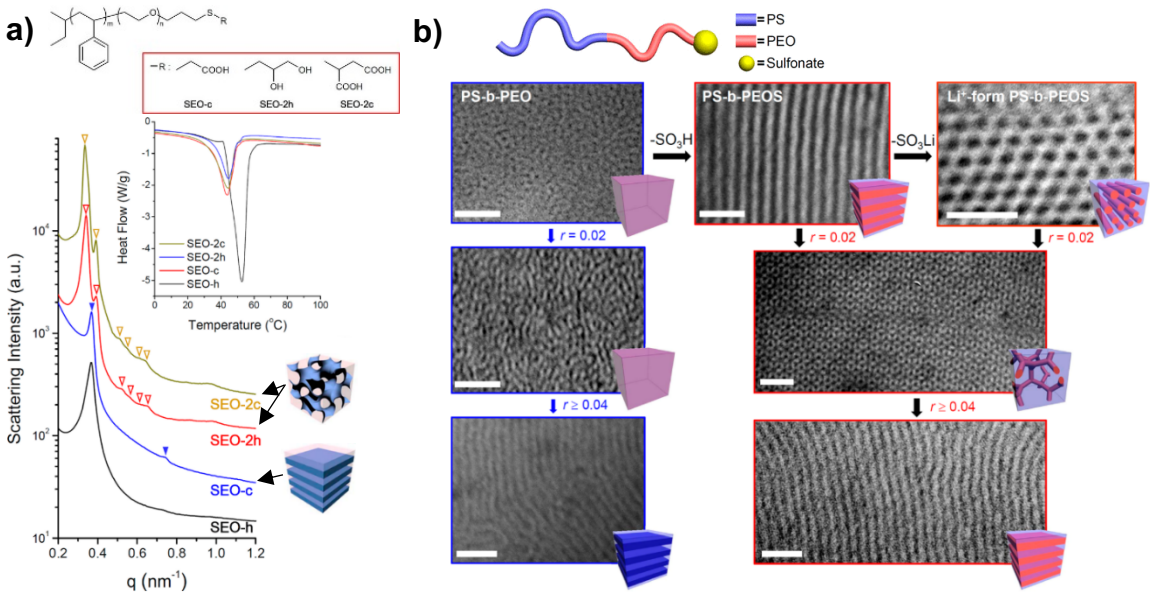

Figure 7. Comparing the phase behavior of PS-PEO with different terminal functionalities at similar molecular weights and compositions of (a) 13.9 kg/mol, f_{PEO} ~ 0.45 and (b) 10.0 kg/mol, f_{PEO} ~ 0.40. (a) SAXS profiles at 60 °C show how substituting the end-group from mono-functional -OH to di-functional -COOH shifts the resulting morphology from DIS to GYR. Adapted with Permission.[69] Copyright 2017, American Chemical Society. (b) TEM images show how substituting mono-functional -OH to -SO_3H and then to -SO_3Li result in DIS→LAM→HEX morphological transitions respectively. PEO phases were darkened with RuO_4. Reproduced with permission.[148] Copyright 2013, American Chemical Society.

Substantial thermodynamic deviations from neutral BP behavior have been demonstrated by the introduction of just a single, well-placed sulfonate group.[148] Substituting the terminal hydroxyl proton of PS-b-PEO with sulfonic acid induced a well-defined LAM morphology (Figure 7b), equivalent to a LiTFSI loading of r = 0.06 in their control (terminal hydroxyl) BPE. Exchanging the acidic proton (SO_3H) with Li (SO_3Li) induced yet another transition from LAM to HEX which was attributed to a decrease in PEO volume fraction and hypothesized to be caused by a reduction in free volume due to the replacement of H-bond interactions with Coulombic interactions. Subsequent doping with LiTFSI lead to a non-monotonic trend in domain spacing with an initial decrease at r = 0.02 followed by an increase at r = 0.06 which constituted a HEX→GYR→LAM series of OOTs. This trend was attributed to strong electrostatic attractions between Li salts and Li sulfonate groups which were screened at higher concentrations as salts entropically distributed throughout the PEO domain. Figure 7 compares the impact of terminal functionality on the phase behavior of similar PS-PEO BPs at near symmetric compositions with -SO_3Li resulting in a more asymmetric shift in phase behavior. It would be interesting to see if

converting -COOH in Figure 7a to -COOLi would produce the same effects as that of -SO_3Li in Figure 7b. Terminal functionalization is a powerful tool as it strategically positions that functionality at the most dynamic segment of the polymer. Kim et al. has recently compiled a review on end-group chemistries and the resulting thermodynamic impact within several polymeric systems.[149]

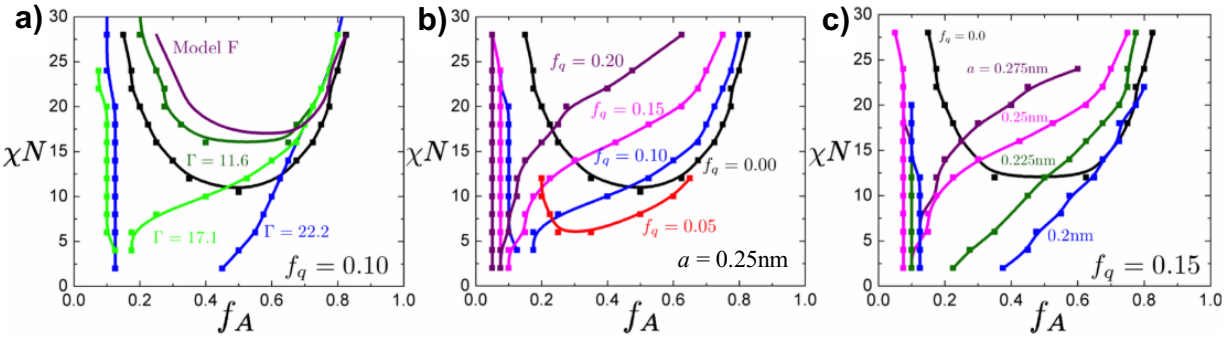

Figure 8. Theoretical SCFT-LS calculations for charge-neutral BPs illustrate shifts in the ODT boundary with respect to (a) Γ which represents electrostatic interaction stength, (b) charge fraction (f_q), and (c) ion radius (a) where f_A is volume fraction of the charged block. Black curves represent the neutral case where $f_q = 0$. Reproduced with permission.[93] Copyright 2015, AIP Publishing.

To help elucidate the effects of strong electrostatic correlations on charge-neutral polymer blends[150,151] and charge-neutral diblock copolymers,[93,129] Sing and Olvera de la Cruz developed a hybrid self-consistent field theory-liquid state theory (SCFT-LS) which considers electrostatic correlations on a local (<10 nm) level while maintaining mean field approximations at larger length scales (10-100 nm). Their work showed that a linear relationship between χ_{eff} and charge fraction (i.e. vertical χN shifts) can be described by ion entropy and solubility effects alone. However, taking into consideration the strongly coupled, cohesive interactions between charged species can lead to a funneling of ordered phases towards low χN and volume fractions of the charged block (Figure 8), even when differences in ion solubility between phases are null (i.e. $\varepsilon_A \sim \varepsilon_B$). A unitless term used to describe this cohesive energy was defined as $\Gamma = l_B/d = e^2/4\pi\varepsilon_0\varepsilon_r k_B T d$ which is the Bjerrum length (l_B) normalized by the ion-counterion pair distance (d), where k_B is the Boltzmann constant, T is temperature, e is the electric charge, and ε_0 and ε_r are the vacuum and relative permittivity, respectively. Shown in Figure 8a are the theoretical effects of Γ on the phase diagram for BPEs with dielectrically equivalent blocks ($\varepsilon_{r,A} = \varepsilon_{r,B}$) where phase separation is suppressed by counterion entropy at low Γ and dictated by charge cohesion at

higher Γ.[93,129] The trends in Figure 8a are the result of varying dielectric permittivity in Γ. The effects of charge fraction (f_q = mole fraction charged monomers in block A) (Figure 8b) are shown alongside the effects of ion-counterion pair distance ($2a$), where a is the effective radius for the ion and counterion. Increasing ion pair spacing (i.e., larger ions) in all but the lowest charged block compositions consistently results in a reduction in phase separation which coincides with an increased tendency towards phase inversion provoked by entropic excluded volume effects. Simply, this means that larger ion spacings exacerbate the funneling effect while also increasing miscibility along most of the compositional axis. A less consistent trend is observed with respect to charge fraction (f_q). For example, a symmetric composition where an initial χ_{eff} enhancement at low f_q is offset by excluded volume penalties at higher f_q (representative of increasing the free energy of the ordered state) would consequently lead to reentrant phase behavior (i.e. DIS→Order→DIS) with increasing f_q. To our knowledge, reentrant phase behavior as a function of salt content in BPEs has only been observed in one instance for asymmetric LiTFSI doped PS-PEO where DIS→weakly-ordered BCC→DIS→HEX transitions occurred with increasing salt content.[113] In another unique instance, LAM→CYL→LAM→CYL alternating morphologies were observed by Sloan et al. upon increasing the protonation level of poly(2-vinylpyridine)-poly(oligoethylene glycol methyl ether methacrylate).[96] In both studies, these unexpected transitions occurred for a single sample within a very narrow parameter range. Further work will be needed to establish a reproducible trend and to identify the underlying mechanism. Temperature-dependent reentry in BPEs with multiple secondary interactions has also been observed recently and will be discussed in the following section (3.2.2).

The extent to which this funneling effect is currently illustrated by the SCFT-LS model[93,129] has not been fully realized experimentally for BPEs. One factor which might help align theoretical predictions via this model with experiment findings is a consideration of composition fluctuations. Composition fluctuations theoretically describe the inconsistency in composition between each BP chain that exist in every experimental BP system since not every polymer chain comprises the exact same composition, regardless of how close the dispersity is to unity for each block. Composition fluctuations have been shown to suppress ordering, a phenomenon which exacerbates as molecular weight decreases.[122,124,125] It is also important to note that the greater the dispersity is for each block, the greater the composition fluctuations will be. To our

knowledge, the closest experiments have come to the ordered, narrow-channel regime depicted in Figure 8 (e.g. Figure 8b, $f_A = 0.1$, $\chi N \sim 7.5$) has been work produced by Winey and coworkers where highly ordered and periodic morphologies were obtained from step-growth polymers with precisely controlled polyethylene spacers separating polar sulfonate moieties.[152–156] Each polyethylene spacer contains exact values of repeat units while polar segments contain only a

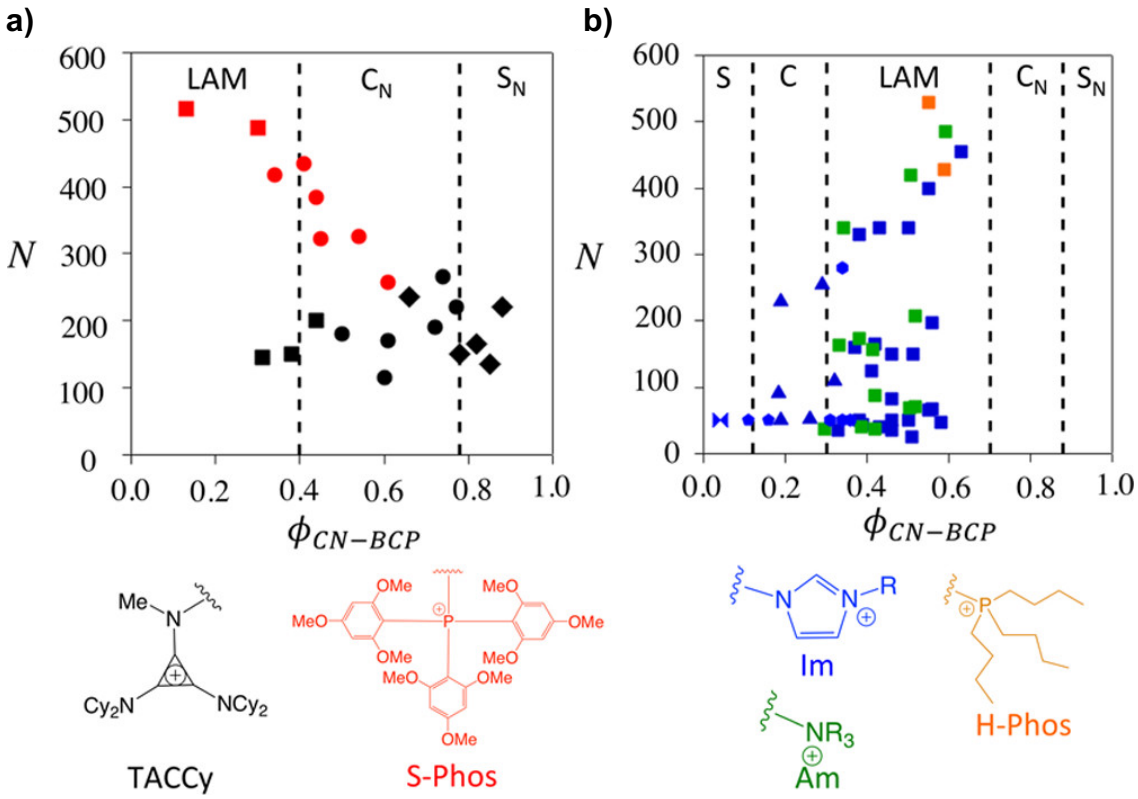

Figure 9. Morphologies of styrenic charge-neutral block copolymers (CN-BPs) mapped onto phase diagrams by degree of polymerization (N) and charged block volume fraction ($\phi_{CN\text{-}BP}$). Pendant cations comprising the charged black are: (a) Trisaminocyclopropenium cyclohexane (TACCy, black)[157] and tris(2,4,6-trimethoxyphenyl)-phosphonium (S-Phos, red)[160] which result in phase asymmetry while (b) alkyl imidazolium (Im, blue), quaternary ammonium (Am, green), and tributylphosphonium (H-Phos, orange) do not result in phase asymmentry.[97,166–169] (squares = LAM, hexagons = LAM/ C, triangles = C, pentagons = S, and bowtie = disordered). Peproduced with permission.[157] Copyright 2020, American Chemical Society

single sulfonate group, resulting in a "block" polymer which effectively nullifies the existence of composition fluctuations. In recent work, HEX→LAM morphologies at $f_{polar} = 0.16$ were observed which constitutes a significant horizontal shift in ordered phases.

Russel et al. observed significant phase asymmetry towards low charge compositions in a styrenic system with bulky trisaminocyclopropenium (TACCy) pendant charges (Figure 9a) where Γ is expected to be high due to the low permittivity of PS.[157]Additionally, the unconventionally low dielectric permittivity calculated ($\varepsilon_r \approx 2.5\text{-}3.0$) for the BPE was believed to contribute significantly to electrostatic cohesion due to the fact that it would increase the Bjerrum length, thus further increasing Γ. Domain spacing (D) and degree of polymerization (N) were found to be proportional ($D \propto N$) which signifies a highly extended, rodlike conformation. For comparison; D scales as $N^{1/2}$ in the weak segregation limit and $N^{2/3}$ in the strong segregation limit (for $N >> 10$) for neutral BPs.[158] The combination of a stiff, styrenic backbone along with large, planar charge moieties points towards low configurational entropy which likely promotes chain extension. Additionally, the TAC-type cations used in this study have been shown to preferentially coordinate to one another rather than to the surrounding counterions. This consequently produces strong stacking arrangements which lack interposing counterions (located radially) and are dominated by dispersion forces whose interplanar distance is akin to neutral π-stacked arenes.[159] This stacking behavior would only further instigate chain stretching. Using a simple geometric scaling model, they concluded that a balance between surface tension and electrostatic repulsion between cations at the interface may play a role in stabilizing charged matrix morphologies for this system (Figure 9a). The addition of LiTFSI salts was able to relax chain extension via charge screening as shown by a decrease in domain spacing. Equilibrium thermodynamics were however, brought into question. They annealed for 1 week at 150 °C (supposedly T_g + 20 °C), the true equilibrium nature of the system was noted as being unclear, since terminal annealing temperatures (generally T_g + 50 °C, Vogel temperature) succeeded the onset of degradation (160 °C). No description of T_g characterization or reference was provided. A previous study by Jiang et al. characterized the same polymer and measured no T_g before degradation.

Zhang and Coughlin also observed substantial phase asymmetry, along with a high degree of chain stretching ($D \propto N$) for diblock and triblock BPEs where very bulky, tris(2,4,6-trimethoxyphenyl)phosphonium Cl pendant ions (Figure 9a, red) constituted the charges along the styrenic backbone of PS-b-PI diblock and PI-b-PS-b-PI triblock copolymers.[160] The bulky trimethoxyphenyl side groups, along with the larger phosphonium ion (relative to ammonium)

likely promote excluded volume effects which would thus encourage horizontal shifts; however, the mechanisms controlling phase asymmetry in this system remain unclear. Phase asymmetry was more evident in the diblock than in the triblock system. OOTs tend to shift towards lower compositions of the terminal blocks of triblock copolymers,[102] which were neutral PI in this case. Hence, architectural effects may have slightly offset the phase asymmetry induced by strong electrostatic cohesion in the midblock. Competing architectural factors such as this could prove to be an interesting route for increasing charged volume fraction while maintaining a desired morphology, in other words by limiting the asymmetric shift. The ionic conductivity was however exceptionally higher in the diblock system, likely due to its charged matrix HEX morphology whereas the triblock formed LAM, which hinders ion transport due to the formation of grain boundaries.[70,161] One takeaway from these two studies is that bulky pendant charges can greatly elongate the chain conformation which then promotes phase asymmetry/inversion.

3.2.2. Boundary inversion

Boundary inversion (defined in section 3.2) describes the change in phase behavior from mixing with increasing temperature (UODT) to mixing with decreasing temperature (LDOT). Boundary inversion is seldomly observed and can be caused by several factors, including volume reduction upon mixing, mismatch in pure component free volume or compressibility, or competitive interactions with different temperature dependencies. When multiple interactions exist, ΔS_{mix} generally remains positive as is typical while ΔH_{mix} can change sign from negative to positive when enthalpic interaction terms have different temperature dependencies. Our focus here will be to describe the few experimental systems which have observed LDOT behavior in strongly interacting BPEs and to form thermodynamic arguments about how each term might be affecting ΔG_{mix}.

To our knowledge, Sloan and Olsen were the first to observe LDOT behavior in solvent-free/bulk BPEs using protonated poly(2-vinylpyridine)-b-POEGMA (P2VP-POEGMA).[96] The neutral blocks are fully miscible within the composition (0.07-0.70) and temperature (40-120 °C) ranges studied but become immiscible upon protonation of the vinylpyridine block with strong acids.[95,96] All protonated samples displayed LDOT behavior wherein increasing acid content from 0-100 mol% in the P2VP block decreased the T_{ODT} (increased χ_{eff}). Although the relative

permittivity of the P2VP phase was less than or equal to that of the POEGMA phase, acid-base interactions with the pyridine group provides a strong "solvation" preference for the acids into the P2VP phase, thus increasing segregation strength. Kinetic restrictions, once again, likely played a role in their observations as it was not possible to anneal above T_g at protonation levels greater than 40% (T_g = 120 °C at 40% protonation). For this reason, all morphological characterizations were conducted by incrementally increasing the temperature from samples solution casted out of water at room temperature. Regardless, consistent trends were observed. The phase diagram remained relatively symmetric, with protonation level being more comparable to salt doped BPEs dominated by solvation effects than to those more dominated by electrostatic cohesion. However, the HEX morphology was suppressed at higher charge compositions (f_{P2VP}) with the LAM morphology stabilized in all samples up to f_{P2VP} ~0.72-0.78, although HPL was observed in a few instances at the highest protonation levels and lowest temperatures studied. At the highest protonation level (100%), the HEX morphology was stabilized up to f_{P2VP} = 0.42, which is very unusual and signifies a horizontal shift in ordered phases towards higher charge compositions as opposed to the opposite trend predicted by theory and observed in other BPEs. The reasoning behind the observed LDOT behavior was suggested to manifest from ions segregating into the lower dielectric phase. Since anions and ether groups are repulsive towards each other, it can be assumed that the driving force behind the LDOT behavior was a result of pyridinium-ether interactions which may be more dominated by H-bonding rather than electrostatics.

Wang and Fan developed two unique BPE systems where boundary inversion can be intricately tuned via a balance of competitive H-bonding and electrostatic interactions.[76,162–164] The first system is $LiClO_4$-doped poly(ethylene oxide)-b- poly(tert-butyl acrylate-co-acrylic acid) (Figure 10c). Increased miscibility due to H-bonding between opposing blocks results in a disorder-to-order transition (DOT) upon heating. Salt-doping can increase segregation via preferential ion solvation.[76] Increasing temperature further resulted in an ODT (i.e., closed-loop phase behavior), representative of a system with positive ΔS_{mix}. The thermodynamic description detailed by the authors goes as follows: The Gibbs free energy of mixing (ΔG_{mix}) can be written as $\Delta G_{mix} = \Delta H_V + \Delta H_C + \Delta H_H - T\Delta S_{mix}$ where the enthalpy of mixing (ΔH_{mix}) is a sum of the vdW (V), Coulombic (C), and H-bonding (H) contributions while the mixing entropies are encapsulated into a single term (ΔS_{mix}) which remains positive along with ΔH_V and ΔH_C. ΔH_H is

negative, however, and its absolute value decreases quicker than $\Delta H_V+\Delta H_C$ since H-bonding strength weakens more quickly than Coulombic strength with respect to increasing temperature. Hence, as temperature increases, ΔH_{mix} flips from being negative to being positive which contributes to miscibility and immiscibility, respectively. It was expected that the entropic term would eventually dominate ($\Delta H_{mix} - T\Delta S_{mix} < 0$) at even higher temperatures to result in mixing and was evidenced by the single instance of closed-loop behavior. Increasing salt content causes ΔH_C to become more positive due to preferential ion solvation into the PEO phase in addition to interfering with H-bonding through Li-ether complexation, which in turn decreases the lower disorder-to-order transition temperature (T_{DOT}) and increases the upper order-to-disorder transition temperature (T_{ODT}).

A second BPE developed by the Wang and Fan consists of an alkyl imidazolium pendant acrylate backbone (PAOEMIm-X) polymerized from a PEO block and illustrated in Figure 10a below. H-bonding in this system originates from protons within the imidazolium rings rather than acidic groups in the previous system (Figure 10c). Weakening of the H-bonding interactions between imidazolium and ether groups with increasing temperature was noted to cause the LDOT behavior. This observation was supported both by FT-IR spectroscopy measurements and by the fact that mixtures of PEO in imidazolium ILs also display LCST behavior which is highly dependent on H-bonding.[165] This also suggests that LDOT behavior observed in protonated

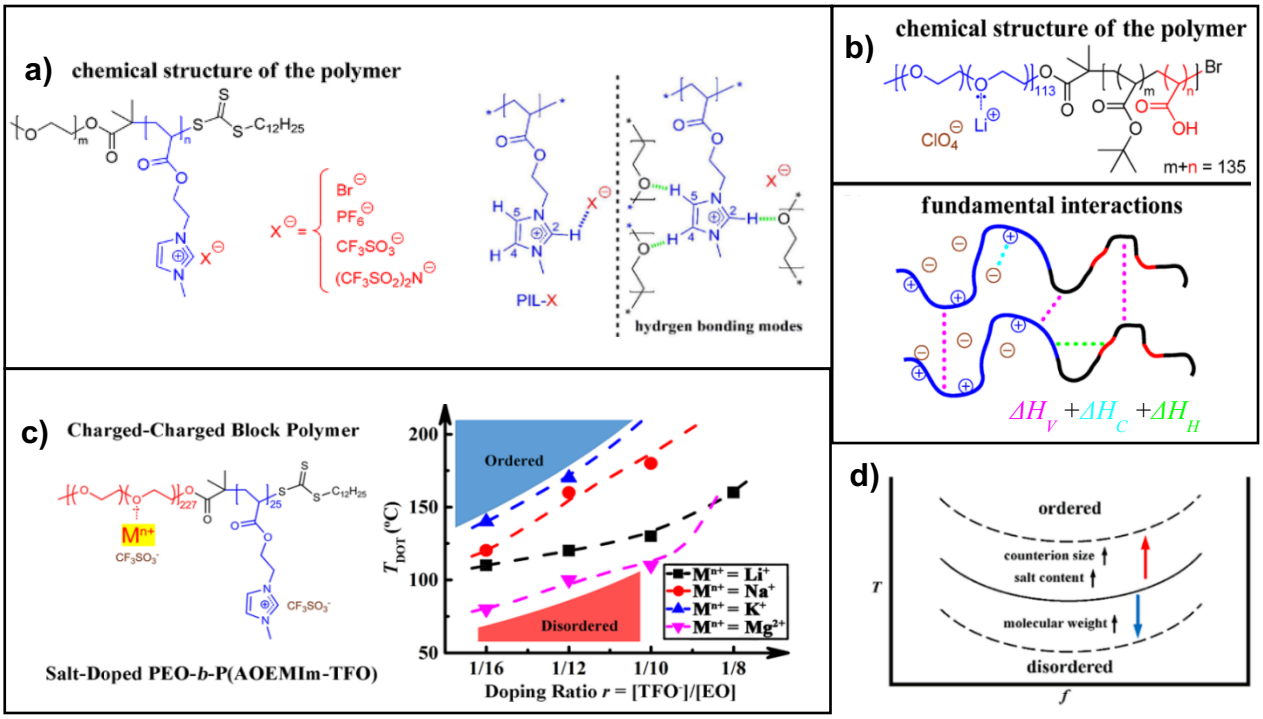

Figure 10. (a) Chemical structure of poly(ethylene oxide)-b-poly(1-((2- acryloyloxy)ethyl)-3-methylimidazolium) with X counterion (PEO-b-PAOEMIm-X) with a depiction of H-bonding interactions between imidazolium rings, anions, and ether segments. Adapted with permission.[163] Copyright 2018, American Chemical Society. (b) Chemical structure of $LiClO_4$-doped poly(ethylene oxide)-b-poly(tert-butyl acrylate-co-acrylic acid) (PEO-b-P(tBA-co-AA)) and depiction of fundamental enthalpic vdW, coulombic, and H-bonding interactions. Adapted with permission.[76] Copyright 2018, American Chemical Society. (c) Chemical structure of salt-doped PEO-b-PAOEMIm-TFO with its T_{DOT} dependence on salt content and cation type. Adapted with permission.[162] Copyright 2018, American Chemical Society (d) Methods for controlling T_{DOT} for the systems displayed in (a) and (c). Adapted with permission.[163] Copyright 2020, American Chemical Society.

P2VP-POEGMA by Sloan et al. may be more dependent on H-bonding rather than Coulombic interactions.[96] Considerable phase asymmetry was also observed with ordered morphologies favoring lower charge compositions and was most evident in samples with smaller counterions. With bromide counterions, LAM appeared at $f_{PAOEMIm\text{-}Br} = 0.26$ and an inverse HEX at $f_{PAOEMIm\text{-}Br} = 0.47$. Phase asymmetry seems to be unique to the system depicted in Figure 10a as it is not generally evident in other imidazolium pendant BPEs, regardless of counterion size.[87,166,167] For the system in Figure 10a, increasing the imidazolium counterion size suppressed asymmetry and increased miscibility due to a reduction in Coulombic strength and increased anion solvation. Doping with Li-CF_3SO_3 (Li-TfO) also increased miscibility due to competing solvation effects between phases and was further exacerbated by increasing the cation size of the salt, although

using a divalent cation (Mg^{2+}) produced the opposite effect due to ionic cross-linking (Figure 10c).[162] The morphological complexity of this BPE has recently been intensified by increasing the alkyl substituent length on the imidazolium ring, leading to a 3-level hierarchical structure with a liquid crystalline mesophase.[164]

4. Future Perspective

Charged BPs offer design solutions for an array of applications in energy storage and conversion, although the unique ability of charges to skew the location, size, and shape of ordered morphologies within the block polymer phase diagram may very well expand the list of potential applications. Understanding the role that electrostatic interactions play in the overall thermodynamics of charge block polymer assembly is of focal importance in the design and development of advanced soft material technologies.

We have highlighted several strategies which can be used to tune the morphology and improve the performance (most commonly ion transport and/or mechanical properties) of charged block polymers. Examples include nanoscale confinement of charges, interfacial segment/block tapering, end-group functionality, support phase chemistry, and the covalent or non-covalent immobilization of subordinate ions. The confinement of charges into nanoscale domains can increase charge density (meq charge/volume), which is one unique feature that block polymers offer and is a powerful approach to lowering the activation barrier for ion transport. Introducing tapered interfacial segments/blocks can stabilize matrix morphologies desirable in electrolytic applications, such as the gyroid phase (i.e., bicontinuous networks) which is relevant to applications beyond those for lithium-ion batteries. Since block tapering also reduces T_{ODTS}, it could also prove useful for studying systems with strong electrostatic interactions where the attainment of equilibrium morphologies is impeded by thermal degradation. End-group functionalization introduces tunability to one of the most dynamic segments of a polymer chain, and thus affords a high degree of control over morphological and interfacial characteristics. The implications that end-group functionalization could have on electrochemical applications continues to be a prominent area of research. Covalent isolation of subordinate ions into the mechanical support phase to produce single-ion conductors has improved transference of the

primary ion while consequently promoting phase mixing due to strong ion-pair dissociation interactions. The introduction of another neutral block or the reduction of charge fraction within the support block might alleviate some of the mixing interactions associated with anti-preferential solvation of counterions into the opposing phase. Coercion of anions into the support phase via hydrogen bonding is a rather nascent technique utilized in cation electrolytes. It is a promising and relatively simple technique which can be better understood by tuning parameters such as the acidity, location, and density of hydrogen bond donors. Could we also find anions which are more susceptible to hydrogen bonding, and would this improve performance?

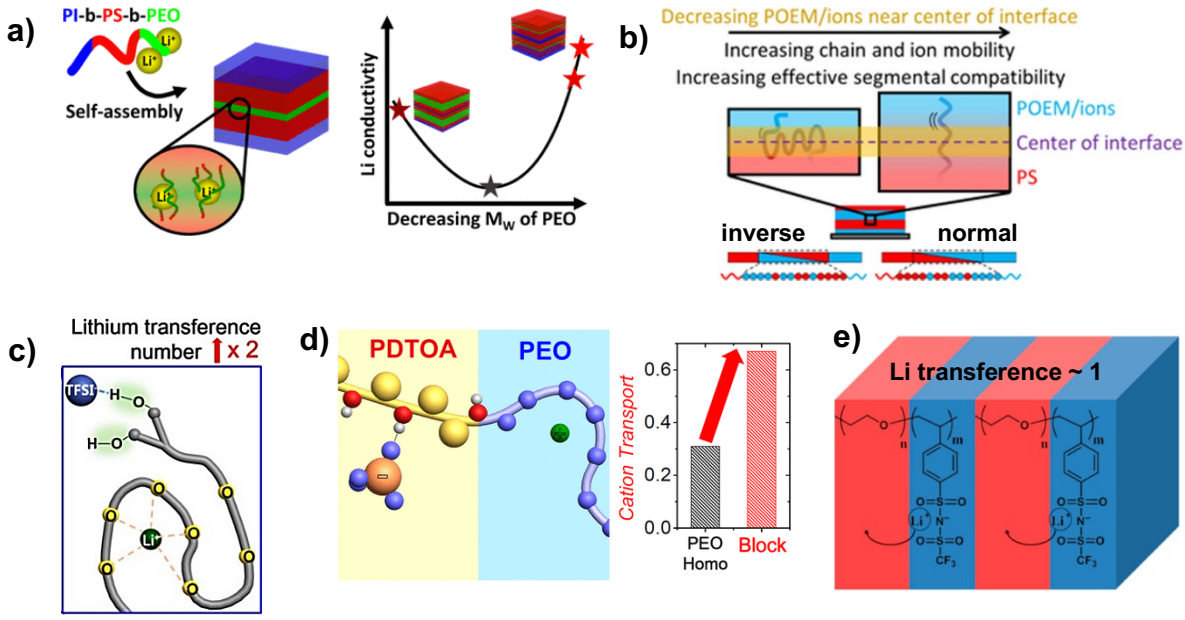

Figure 11. Summary of tunable factors discussed in this review that have been shown to improve and/or have potential to improve the performance of BCEs. (a) Nano-confinement of ionic domains, Adapted with permission.[62] Copyright 2019, American Chemical Society. (b) Interfacial tapering. Adapted with permission.[67] Copyright 2021, American Chemical Society. (c) Terminal functionalization. Adapted with permission.[69] Copyright 2017, American Chemical Society. (d) Coercion of subordinate ions into the support phase via non-bonded interactions. Adapted with permission.[75] Copyright 2015, American Chemical Society. (e) Covalent tethering of subordinate ions onto the support block to produce single-ion conductors. Adapted with permission.[79] Copyright 2014, American Chemical Society.

The isolation of parameters associated with ion thermodynamics is critical for the field to improve our understanding of the impact of electrostatic interactions on the overall thermodynamics of block polymers. Varying the linker spacing between pendant charges and the backbone, in addition to the immobilization of counterions (i.e., formation of zwitterions) are

two approaches which could further illuminate the impacts of ion translational entropy. The direct comparison between small, bulky, and liquid-type charge moieties along the same backbone would expose the enthalpic relationships and differences between them. Guided by theory and scrutinized by experimentation, we will continue to elucidate the intricate nature of electrostatics and the relationship it has with morphology and material performance.

Acknowledgements

The authors would like to thank the National Science Foundation for supporting this work through Grant No. 1848454.

References

[1] W. S. Young, W. F. Kuan, T. H. Epps, *J. Polym. Sci. Part B: Polym. Phys.* **2014**, *52*, 1.
[2] T. Liu, G. Liu, *J. Phys.: Condens. Matter* **2019**, *31*.
[3] K. M. Diederichsen, E. J. McShane, B. D. McCloskey, *ACS Energy Lett.* **2017**, *2*, 2563.
[4] Y. A. Elabd, M. A. Hickner, *Macromolecules,* **2011**, *44*, 1.
[5] H. A. Elwan, R. Thimmappa, M. Mamlouk, K. Scott, *J. Power Sources* **2021**, *510*, 230371.
[6] L. Wu, Z. Zhang, J. Ran, D. Zhou, C. Li, T. Xu, *Phys. Chem. Chem. Phys.* **2013**, *15*, 4870.
[7] C. Feng, C. P. Hemantha Rajapaksha, A. Jákli, *Engineering* **2021**, *7*, 581.
[8] M. D. Green, T. E. Long, *Polym. Rev.,* **2009**, *49*, 291.
[9] M. D. Green, D. Wang, S. T. Hemp, J. H. Choi, K. I. Winey, J. R. Heflin, T. E. Long, *Polymer* **2012**, *53*, 3677.
[10] A. J. Duncan, D. J. Leo, T. E. Long, *Macromolecules* **2008**, *41*, 7765.
[11] A. J. Duncan, B. J. Akle, T. E. Long, D. J. Leo, *Smart Mater. Struct.* **2009**, *18*, 104005.
[12] M. D. Bennett, D. J. Leo, *Sens. Actuators A* **2004**, *115*, 79.
[13] S. Liu, W. Liu, Y. Liu, J. H. Lin, X. Zhou, M. J. Janik, R. H. Colby, Q. Zhang, *Polym. Int.* **2010**, *59*, 321.
[14] B. J. Akle, D. J. Leo, M. A. Hickner, J. E. McGrath, *J. Mater. Sci.* **2005**, *40*, 3715.
[15] B. J. Akle, M. D. Bennett, D. J. Leo, *Sens. Actuators A* **2006**, *126*, 173.
[16] Y. Yang, T. L. Ramos, J. Heo, M. D. Green, *J. Membr. Sci.* **2018**, *561*, 69.
[17] E. R. Thomas, A. Jain, S. C. Mann, Y. Yang, M. D. Green, W. S. Walker, F. Perreault, M. L. Lind, R. Verduzco, *J. Membr. Sci.* **2020**, *613*, 118460.
[18] Y. Zhang, Y. Liu, B. Ren, D. Zhang, S. Xie, Y. Chang, J. Yang, J. Wu, L. Xu, J. Zheng, *J. Phys. D: Appl. Phys.* **2019**, *52*, 403001.
[19] S. P. Nunes, *Macromolecules* **2016**, *49*, 2905.
[20] X. Shi, H. Xiao, H. Azarabadi, J. Song, X. Wu, X. Chen, K. S. Lackner, *Angew. Chem.* **2020**, *132*, 7048.

[21] N. S. Schauser, A. Nikolaev, P. M. Richardson, S. Xie, K. Johnson, E. M. Susca, H. Wang, R. Seshadri, R. J. Clément, J. Read De Alaniz, R. A. Segalman, *ACS Macro Lett.* **2021**, *10*, 104.
[22] J. A. Bollinger, M. J. Stevens, A. L. Frischknecht, *ACS Macro Lett.* **2020**, *9*, 583.
[23] D. M. Pesko, M. A. Webb, Y. Jung, Q. Zheng, T. F. Miller, G. W. Coates, N. P. Balsara, *Macromolecules* **2016**, *49*, 5244.
[24] S. Stalin, S. Choudhury, K. Zhang, L. A. Archer, *Chem. Mater.* **2018**, *30*, 2058.
[25] D. Zhang, X. Xu, Y. Qin, S. Ji, Y. Huo, Z. Wang, Z. Liu, J. Shen, J. Liu, *Chem. - Eur. J.* **2020**, *26*, 1720.
[26] F. S. Bates, G. H. Fredrickson, *Phys. Today* **1999**, *52*, 32.
[27] G. S. Doerk, K. G. Yager, *Mol. Syst. Des. Eng.* **2017**, *2*, 518.
[28] H. C. Kim, S. M. Park, W. D. Hinsberg, I. R. Division, *Chem. Rev.* **2010**, *110*, 146.
[29] B. A. Paren, *PhD Thesis*, University of Pennsylvania, **2021**.
[30] A. S. Shaplov, R. Marcilla, D. Mecerreyes, *Electrochim. Acta* **2015**, *175*, 18.
[31] P. M. Ketkar, K. H. Shen, L. M. Hall, T. H. Epps, *Mol. Syst. Des. Eng.* **2019**, *4*, 223.
[32] T. Ito, G. Ghimire, *ChemElectroChem* **2018**, *5*, 2937.
[33] K. M. Meek, Y. A. Elabd, *J. Mater. Chem. A* **2015**, *3*, 24187.
[34] R. K. Nagarale, G. S. Gohil, V. K. Shahi, *Adv. Colloid Interface Sci.* **2006**, *119*, 97.
[35] M. A. Hickner, H. Ghassemi, Y. S. Kim, B. R. Einsla, J. E. McGrath, *Chem. Rev.* **2004**, *104*, 4587.
[36] D. T. Hallinan, N. P. Balsara, *Annu. Rev. Mater. Res.* **2013**, *43*, 503.
[37] J. Mindemark, M. J. Lacey, T. Bowden, D. Brandell, *Prog. Polym. Sci.* **2018**, *81*, 114.
[38] M. J. Park, *Mol. Syst. Des. Eng.* **2019**, *4*, 239.
[39] V. Ganesan, *Mol. Syst. Des. Eng.* **2019**, *4*, 280.
[40] J. S. Lee, A. Hocken, M. D. Green, *Mol. Syst. Des. Eng.* **2021**, *6*, 334.
[41] M. D. Galluzzo, W. S. Loo, A. A. Wang, A. Walton, J. A. Maslyn, N. P. Balsara, *J. Phys. Chem. B* **2020**, *124*, 921.
[42] D. Golodnitsky, E. Strauss, E. Peled, S. Greenbaum, *J. Electrochem. Soc.* **2015**, *162*, A2551.
[43] J. A. Maslyn, W. S. Loo, K. D. McEntush, H. J. Oh, K. J. Harry, D. Y. Parkinson, N. P. Balsara, *J. Phys. Chem.C* **2018**, *122*, 26797.
[44] C. Brissot, M. Rosso, J.-N. Chazalviel, S. Lascaud, *J. Power Sources* **1999**, *81–82*, 925.
[45] P. Barai, K. Higa, V. Srinivasan, *Phys. Chem. Chem. Phys.* **2017**, *19*, 20493.
[46] K. Kerman, A. Luntz, V. Viswanathan, Y.-M. Chiang, Z. Chen, *J. Electrochem. Soc.* **2017**, *164*, A1731.
[47] T. Famprikis, P. Canepa, J. A. Dawson, M. S. Islam, C. Masquelier, *Nat. Mater.* **2019**, *18*, 1278.
[48] H. Liu, X. B. Cheng, J. Q. Huang, H. Yuan, Y. Lu, C. Yan, G. L. Zhu, R. Xu, C. Z. Zhao, L. P. Hou, C. He, S. Kaskel, Q. Zhang, *ACS Energy Lett.* **2020**, *5*, 833.
[49] X. Yan, F. Zhang, H. Zhang, H. Tang, M. Pan, P. Fang, *ACS Appl. Mater. Interfaces* **2019**, *11*, 6111.
[50] Y. Li, T. van Cleve, R. Sun, R. Gawas, G. Wang, M. Tang, Y. A. Elabd, J. Snyder, K. C. Neyerlin, *ACS Energy Lett.* **2020**, *5*, 1726.
[51] S. A. Vilekar, R. Datta, *J. Power Sources* **2010**, *195*, 2241.
[52] S. Lascaud, M. Perrier, A. Vallee, S. Besner, J. Prud'homme, M. Armand, *Macromolecules* **1994**, *27*, 7469.

[53] A. Panday, S. Mullin, E. D. Gomez, N. Wanakule, V. L. Chen, A. Hexemer, J. Pople, N. P. Balsara, *Macromolecules* **2009**, *42*, 4632.
[54] M. Chintapalli, T. N. P. Le, N. R. Venkatesan, N. G. Mackay, A. A. Rojas, J. L. Thelen, X. C. Chen, D. Devaux, N. P. Balsara, *Macromolecules* **2016**, *49*, 1770.
[55] M. Singh, O. Odusanya, G. M. Wilmes, H. B. Eitouni, E. D. Gomez, A. J. Patel, V. L. Chen, M. J. Park, P. Fragouli, H. Iatrou, N. Hadjichristidis, D. Cookson, N. P. Balsara, *Macromolecules* **2007**, *40*, 4578.
[56] S. Sharick, J. Koski, R. A. Riggleman, K. I. Winey, *Macromolecules* **2016**, *49*, 2245.
[57] J. Shi, C. A. Vincent, *Solid State Ionics* **1993**, *60*, 11.
[58] D. Sharon, P. Bennington, M. Dolejsi, M. A. Webb, B. X. Dong, J. J. De Pablo, P. F. Nealey, S. N. Patel, *ACS Nano* **2020**, *14*, 8902.
[59] R. Yuan, A. A. Teran, I. Gurevitch, S. A. Mullin, N. S. Wanakule, N. P. Balsara, *Macromolecules* **2013**, *46*, 914.
[60] Y. H. Lin, *Macromolecules* **1990**, *23*, 5292.
[61] T. S. Dörr, A. Pelz, P. Zhang, T. Kraus, M. Winter, H. D. Wiemhöfer, *Chem. - Eur. J.* **2018**, *24*, 8061.
[62] A. Pelz, T. S. Dörr, P. Zhang, P. W. de Oliveira, M. Winter, H. D. Wiemhöfer, T. Kraus, *Chem. Mater.* **2019**, *31*, 277.
[63] K. Timachova, H. Watanabe, N. P. Balsara, *Macromolecules* **2015**, *48*, 7882.
[64] D. Bresser, S. Lyonnard, C. Iojoiu, L. Picard, S. Passerini, *Mol. Syst. Des. Eng.* **2019**, *4*, 779.
[65] W. F. Kuan, R. Remy, M. E. Mackay, T. H. Epps, *RSC Adv.* **2015**, *5*, 12597.
[66] W. F. Kuan, E. H. Reed, N. A. Nguyen, M. E. Mackay, T. H. Epps, *MRS Commun.* **2015**, *5*, 251.
[67] P. M. Ketkar, K.-H. Shen, M. Fan, L. M. Hall, T. H. Epps, *Macromolecules* **2021**, *54*, 7590.
[68] P. M. Ketkar, T. H. Epps, *Acc. Chem. Res.* **2021**, *54*, 4342.
[69] H. Y. Jung, P. Mandal, G. Jo, O. Kim, M. Kim, K. Kwak, M. J. Park, *Macromolecules* **2017**, *50*, 3224.
[70] M. Chintapalli, X. C. Chen, J. L. Thelen, A. A. Teran, X. Wang, B. A. Garetz, N. P. Balsara, *Macromolecules* **2014**, *47*, 5424.
[71] J. Kim, K.-J. Jeong, K. Kim, C. Y. Son, M. J. Park, *Macromolecules* **2022**, *55*, 2028.
[72] X. H. Cao, J. H. Li, M. J. Yang, J. L. Yang, R. Y. Wang, X. H. Zhang, J. T. Xu, *Macromol. Rapid Commun.* **2020**, *41*, 1.
[73] X. H. Cao, J. L. Yang, R. Y. Wang, X. H. Zhang, J. T. Xu, *Polymer* **2019**, *180*.
[74] W. M. Ren, T. J. Yue, M. R. Li, Z. Q. Wan, X. B. Lu, *Macromolecules* **2017**, *50*, 63.
[75] G. Jo, H. Jeon, M. J. Park, *ACS Macro Lett.* **2015**, *4*, 225.
[76] R. Y. Wang, J. Huang, X. S. Guo, X. H. Cao, S. F. Zou, Z. Z. Tong, J. T. Xu, B. Y. Du, Z. Q. Fan, *Macromolecules* **2018**, *51*, 4727.
[77] S.-W. Ryu, P. E. Trapa, S. C. Olugebefola, J. A. Gonzalez-Leon, D. R. Sadoway, A. M. Mayes, *J. Electrochem. Soc.* **2005**, *152*, A158.
[78] R. Bouchet, S. Maria, R. Meziane, A. Aboulaich, L. Lienafa, J. P. Bonnet, T. N. T. Phan, D. Bertin, D. Gigmes, D. Devaux, R. Denoyel, M. Armand, *Nat. Mater.* **2013**, *12*, 452.
[79] S. Inceoglu, A. A. Rojas, D. Devaux, X. C. Chen, G. M. Stone, N. P. Balsara, *ACS Macro Lett.* **2014**, *3*, 510.

[80] A. A. Rojas, S. Inceoglu, N. G. Mackay, J. L. Thelen, D. Devaux, G. M. Stone, N. P. Balsara, *Macromolecules* **2015**, *48*, 6589.
[81] L. Porcarelli, M. A. Aboudzadeh, L. Rubatat, J. R. Nair, A. S. Shaplov, C. Gerbaldi, D. Mecerreyes, *J. Power Sources* **2017**, *364*, 191.
[82] L. Porcarelli, A. S. Shaplov, M. Salsamendi, J. R. Nair, Y. S. Vygodskii, D. Mecerreyes, C. Gerbaldi, *ACS Appl. Mater. Interfaces* **2016**, *8*, 10350.
[83] J. L. Thelen, S. Inceoglu, N. R. Venkatesan, N. G. Mackay, N. P. Balsara, *Macromolecules* **2016**, *49*, 9139.
[84] J. L. Thelen, X. C. Chen, S. Inceoglu, N. P. Balsara, *Macromolecules* **2017**, *50*, 4827.
[85] A. A. Rojas, K. Thakker, K. D. McEntush, S. Inceoglu, G. M. Stone, N. P. Balsara, *Macromolecules* **2017**, *50*, 8765.
[86] D. Devaux, L. Liénafa, E. Beaudoin, S. Maria, T. N. T. Phan, D. Gigmes, E. Giroud, P. Davidson, R. Bouchet, *Electrochim. Acta* **2018**, *269*, 250.
[87] Y. Ye, S. Sharick, E. M. Davis, K. I. Winey, Y. A. Elabd, *ACS Macro Lett.* **2013**, *2*, 575.
[88] K. M. Meek, S. Sharick, Y. Ye, K. I. Winey, Y. A. Elabd, *Macromolecules* **2015**, *48*, 4850.
[89] S. Y. Kim, S. Kim, M. J. Park, *Nat. Commun.* **2010**, *1, 88*.
[90] T. L. Chen, P. M. Lathrop, R. Sun, Y. A. Elabd, *Macromolecules* **2021**, *54*, 8780.
[91] T. L. Chen, R. Sun, C. Willis, B. Krutzer, B. F. Morgan, F. L. Beyer, K. S. Han, V. Murugesan, Y. A. Elabd, *Polymer* **2020**, *209*, 122975.
[92] D. S. la Cruz, M. D. Green, Y. Ye, Y. A. Elabd, T. E. Long, K. I. Winey, *J. Polym. Sci. Part B: Polym. Phys.* **2012**, *50*, 338.
[93] C. E. Sing, J. W. Zwanikken, M. O. de La Cruz, *J. Chem. Phys.* **2015**, *142*, 34902.
[94] O. Kim, K. Kim, U. H. Choi, M. J. Park, *Nat. Commun.* **2018**, *9*, 5029.
[95] C. R. Stewart-Sloan, B. D. Olsen, *ACS Macro Lett.* **2014**, *3*, 410.
[96] C. R. Stewart-Sloan, R. Wang, M. K. Sing, B. D. Olsen, *J. Polym. Sci. Part B: Polym. Phys.* **2017**, *55*, 1181.
[97] G. Sudre, S. Inceoglu, P. Cotanda, N. P. Balsara, *Macromolecules* **2013**, *46*, 1519.
[98] S. A. Mullin, A. A. Teran, R. Yuan, N. P. Balsara, *J. Polym. Sci. Part B: Polym. Phys.* **2013**, *51*, 927.
[99] P. Sutton, P. Bennington, S. N. Patel, M. Stefik, U. B. Wiesner, P. F. Nealey, U. Steiner, I. Gunkel, *Adv. Funct. Mater.* **2019**, *29*, 1905977.
[100] P. v. Truong, R. L. Black, J. P. Coote, B. Lee, H. Ardebili, G. E. Stein, *ACS Appl. Polym. Mater.* **2019**, *1*, 8.
[101] W. Zheng, C. J. Cornelius, *Polymer* **2016**, *103*, 104.
[102] M. W. Matsen, *Macromolecules* **2012**, *45*, 2161.
[103] N. A. Lynd, M. A. Hillmyer, *Macromolecules* **2007**, *40*, 8050.
[104] N. A. Lynd, M. A. Hillmyer, *Macromolecules* **2005**, *38*, 8803.
[105] N. A. Lynd, A. J. Meuler, M. A. Hillmyer, *Prog. Polym. Sci.* **2008**, *33*, 875.
[106] M. W. Matsen, *Phys. Rev. Lett.* **2007**, *99, 148304*.
[107] D. M. Cooke, A. C. Shi, *Macromolecules* **2006**, *39*, 6661.
[108] M. Radhakrishna, C. E. Sing, *Macromol. Chem. Phys.* **2016**, *217*, 126.
[109] A. A. Teran, N. P. Balsara, *J. Phys. Chem. B* **2014**, *118*, 4.
[110] W. S. Loo, G. K. Sethi, A. A. Teran, M. D. Galluzzo, J. A. Maslyn, H. J. Oh, K. I. Mongcopa, N. P. Balsara, *Macromolecules* **2019**, *52*, 5590.

[111] N. S. Wanakule, A. Panday, S. A. Mullin, E. Gann, A. Hexemer, N. P. Balsara, *Macromolecules* **2009**, *42*, 5642.
[112] W. S. Loo, N. P. Balsara, *J. Polym. Sci. Part B: Polym. Phys.* **2019**, *57*, 1177.
[113] W. S. Loo, X. Jiang, J. A. Maslyn, H. J. Oh, C. Zhu, K. H. Downing, N. P. Balsara, *Soft Matter* **2018**, *14*, 2789.
[114] W. S. Loo, M. D. Galluzzo, X. Li, J. A. Maslyn, H. J. Oh, K. I. Mongcopa, C. Zhu, A. A. Wang, X. Wang, B. A. Garetz, N. P. Balsara, *J. Phys. Chem. B* **2018**, *122*, 8065.
[115] G. Zardalidis, K. Gatsouli, S. Pispas, M. Mezger, G. Floudas, *Macromolecules* **2015**, *48*, 7164.
[116] L. Leibler, *Macromolecules* **1980**, *13*, 1602.
[117] W. S. Young, P. J. Brigandi, T. H. Epps, *Macromolecules* **2008**, *41*, 6276.
[118] T. E. Gartner, M. A. Morris, C. K. Shelton, J. A. Dura, T. H. Epps, *Macromolecules* **2018**, *51*, 1917.
[119] K. J. Hou, J. Qin, *Macromolecules* **2018**, *51*, 7463.
[120] K. J. Hou, W. S. Loo, N. P. Balsara, J. Qin, *Macromolecules* **2020**, *53*, 3956.
[121] W. S. Loo, K. I. Mongcopa, D. A. Gribble, A. A. Faraone, N. P. Balsara, *Macromolecules* **2019**, *52*, 8724.
[122] X. Kong, K. J. Y. Hou, J. Qin, *ACS Macro Lett.* **2021**, *10*, 545.
[123] F. S. Bates, M. F. Schulz, A. K. Khandpur, S. Förster, J. H. Rosedale, K. Almdal, K. Mortensen, *Faraday Discuss.* **1994**, *98*, 7.
[124] G. H. Fredrickson, E. Helfand, *The J. Chem. Phys.* **1987**, *87*, 697.
[125] J. Qin, D. C. Morse, *Phys. Rev. Lett.* **2012**, *108*.
[126] J. Huang, Z. Z. Tong, B. Zhou, J. T. Xu, Z. Q. Fan, *Polymer* **2013**, *54*, 3098.
[127] J. Huang, Z. Z. Tong, B. Zhou, J. T. Xu, Z. Q. Fan, *Polymer* **2014**, *55*, 1070.
[128] J. Huang, R. Y. Wang, Z. Z. Tong, J. T. Xu, Z. Q. Fan, *Macromolecules* **2014**, *47*, 8359.
[129] C. E. Sing, J. W. Zwanikken, M. Olvera De La Cruz, *Nat. Mater.* **2014**, *13*, 694.
[130] G. S. MacGlashan, Y. G. Andreev, *Nature* **1999**, *398*, 792.
[131] E. Helfand, Y. Tagami, *The J. Chem. Phys.* **1972**, *56*, 3592.
[132] H. Tang, K. F. Freed, *The J. Chem. Phys.* **1991**, *94*, 6307.
[133] D. J. Grzetic, K. T. Delaney, G. H. Fredrickson, *J. Chem. Phys.* **2018**, *148*, 204903.
[134] D. J. Grzetic, K. T. Delaney, G. H. Fredrickson, *ACS Macro Lett.* **2019**, *8*, 962.
[135] W. F. Kuan, R. Remy, M. E. Mackay, T. H. Epps, *RSC Adv.* **2015**, *5*, 12597.
[136] J. R. Brown, S. W. Sides, L. M. Hall, *ACS Macro Lett.* **2013**, *2*, 1105.
[137] J. Shim, F. S. Bates, T. P. Lodge, *ACS Macro Lett.* **2019**, *8*, 1166.
[138] J. Shim, F. S. Bates, T. P. Lodge, *Nat. Commun.* **2019**, *10, 2108*.
[139] B. Zhang, C. Zheng, M. B. Sims, F. S. Bates, T. P. Lodge, *ACS Macro Lett.* **2021**, *10*, 1035.
[140] M. W. Matsen, *Macromolecules* **1995**, *28*, 5765.
[141] M. W. Matsen, *Phys. Rev. Lett.* **1995**, *74*, 4225.
[142] K. I. Winey, E. L. Thomas, L. J. Fetters, *Macromolecules* **1991**, *24*, 6182.
[143] M. J. Park, N. P. Balsara, *Macromolecules* **2008**, *41*, 3678.
[144] M. Goswami, B. G. Sumpter, T. Huang, J. M. Messman, S. P. Gido, A. I. Isaacs-Sodeye, J. W. Mays, *Soft Matter* **2010**, *6*, 6146.
[145] H. Y. Jung, S. Y. Kim, O. Kim, M. J. Park, *Macromolecules* **2015**, *48*, 6142.
[146] J. Min, D. Barpuzary, H. Ham, G. C. Kang, M. J. Park, *Acc. Chem. Res.* **2021**, *54*, 4024.

[147] J. Min, H. Y. Jung, S. Jeong, B. Lee, C. Y. Son, M. J. Park, *Proc. Natl. Acad. Sci. U. S. A.* **2021**, *118*.
[148] G. Jo, H. Ahn, M. J. Park, *ACS Macro Lett.* **2013**, *2*, 990.
[149] J. Kim, H. Y. Jung, M. J. Park, *Macromolecules* **2020**, *53*, 746.
[150] C. E. Sing, J. W. Zwanikken, M. O. de La Cruz, *Phys. Rev. Lett.* **2013**, *111*, 1.
[151] C. E. Sing, J. W. Zwanikken, M. Olvera De La Cruz, *ACS Macro Lett.* **2013**, *2*, 1042.
[152] E. B. Trigg, T. W. Gaines, M. Maréchal, D. E. Moed, P. Rannou, K. B. Wagener, M. J. Stevens, K. I. Winey, *Nat. Mater.* **2018**, *17*, 725.
[153] L. Yan, L. Hoang, K. I. Winey, *Macromolecules* **2020**, *53*, 1777.
[154] L. Yan, C. Rank, S. Mecking, K. I. Winey, *J. Am. Chem. Soc.* **2020**, *142*, 857.
[155] B. A. Paren, B. A. Thurston, W. J. Neary, A. Kendrick, J. G. Kennemur, M. J. Stevens, A. L. Frischknecht, K. I. Winey, *Macromolecules* **2020**, *53*, 8960.
[156] J. Park, A. Staiger, S. Mecking, K. I. Winey, *Macromolecules* **2021**, *54*, 4269.
[157] S. T. Russell, R. Raghunathan, A. M. Jimenez, K. Zhang, S. D. Brucks, C. Iacob, A. C. West, O. Gang, L. M. Campos, S. K. Kumar, *Macromolecules* **2020**, *53*, 548.
[158] F. S. Bates, G. H. Fredrickson, *Annu. Rev. Phys. Chem.* **1990**, *41*, 525.
[159] A. J. Wallace, C. D. Jayasinghe, M. I. J. Polson, O. J. Curnow, D. L. Crittenden, *J. Am. Chem. Soc.* **2015**, *137*, 15528.
[160] W. Zhang, Y. Liu, A. C. Jackson, A. M. Savage, S. P. Ertem, T. H. Tsai, S. Seifert, F. L. Beyer, M. W. Liberatore, A. M. Herring, E. B. Coughlin, *Macromolecules* **2016**, *49*, 4714.
[161] W. S. Young, T. H. Epps, *Macromolecules* **2012**, *45*, 4689.
[162] R. Y. Wang, Z. K. Zhang, X. S. Guo, X. H. Cao, T. Y. Zhang, Z. Z. Tong, J. T. Xu, B. Y. Du, Z. Q. Fan, *Macromolecules* **2020**, *53*, 4560.
[163] R. Y. Wang, X. S. Guo, B. Fan, S. F. Zou, X. H. Cao, Z. Z. Tong, J. T. Xu, B. Y. Du, Z. Q. Fan, *Macromolecules* **2018**, *51*, 2302.
[164] Z. K. Zhang, X. S. Guo, T. Y. Zhang, R. Y. Wang, B. Y. Du, J. T. Xu, *Macromolecules* **2020**, *53*, 8714.
[165] H. N. Lee, N. Newell, Z. Bai, T. P. Lodge, *Macromolecules* **2012**, *45*, 3627.
[166] J. H. Choi, Y. Ye, Y. A. Elabd, K. I. Winey, *Macromolecules* **2013**, *46*, 5290.
[167] R. L. Weber, Y. Ye, A. L. Schmitt, S. M. Banik, Y. A. Elabd, M. K. Mahanthappa, *Macromolecules* **2011**, *44*, 5727.
[168] V. F. Scalfani, E. F. Wiesenauer, J. R. Ekblad, J. P. Edwards, D. L. Gin, T. S. Bailey, *Macromolecules* **2012**, *45*, 4262.
[169] P. Cotanda, G. Sudre, M. A. Modestino, X. C. Chen, N. P. Balsara, *Macromolecules* **2014**, *47*, 7540.